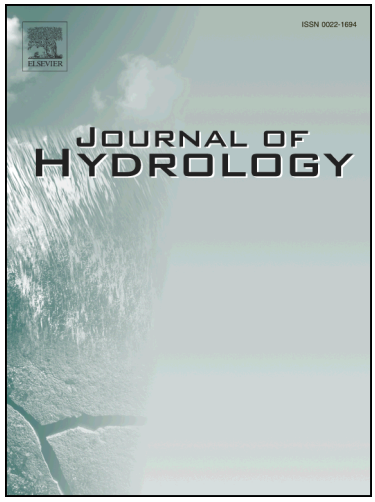

Research papers

Spring Hydrograph Simulation of Karstic Aquifers: Impacts of Variable Recharge Area, Intermediate Storage and Memory Effects

Seiyed Mossa Hosseini, Behzad Ataie-Ashtiani, Craig T. Simmons

PII: S0022-1694(17)30421-3
DOI: http://dx.doi.org/10.1016/j.jhydrol.2017.06.018
Reference: HYDROL 22072

To appear in: *Journal of Hydrology*

Received Date: 12 March 2017
Revised Date: 30 May 2017
Accepted Date: 13 June 2017

Please cite this article as: Hosseini, S.M., Ataie-Ashtiani, B., Simmons, C.T., Spring Hydrograph Simulation of Karstic Aquifers: Impacts of Variable Recharge Area, Intermediate Storage and Memory Effects, *Journal of Hydrology* (2017), doi: http://dx.doi.org/10.1016/j.jhydrol.2017.06.018

Spring Hydrograph Simulation of Karstic Aquifers: Impacts of Variable Recharge Area, Intermediate Storage and Memory Effects

Seiyed Mossa Hosseini [a,*], Behzad Ataie-Ashtiani [b, c], Craig T. Simmons [c]

[a] Natural Geography Department, University of Tehran, P.O. Box 14155-6465, Tehran, Iran.

[b] Department of Civil Eng., Sharif University of Technology, P.O. Box 11155-9313, Tehran, Iran.

[c] National Centre for Groundwater Research & Training and School of the Environment, Flinders University, GPO Box 2100, Adelaide, South Australia 5001, Australia.

Abstract

A simple conceptual rainfall–runoff model is proposed for the estimation of groundwater balance components in complex karst aquifers. In the proposed model the effects of memory length of different karst flow systems of base-flow, intermediate-flow, and quick-flow and also time variation of recharge area (RA) during a hydrological year were investigated. The model consists of three sub-models: soil moisture balance (SMB), epikarst balance (EPB), and groundwater balance (GWB) to simulate the daily spring discharge. The SMB and EPB sub-models utilize the mass conservation equation to compute the variation of moisture storages in the soil cover and epikarst, respectively. The GWB sub-model computes the spring discharge hydrograph through three parallel linear reservoirs for base-flow, intermediate-flow, and quick-flow. Three antecedent recharge indices are defined and embedded in the model structure to deal with the memory effect of three karst flow systems to antecedent recharge flow. The Sasan Karst aquifer located in the semi-arid region of south-west Iran with a continuous long-term (21-years) daily meteorological and discharge data are considered to describe model calibration and validation procedures. The effects of temporal variations of RA of karst formations during the hydrological year namely invariant RA, two RA (winter and summer), four RA (seasonal), and twelve RA (monthly) are assessed to

[*]Corresponding Author. Tel: +98 216 111 3538. *E-mail Address*: smhosseini@ut.ac.ir (S. M. Hosseini).

determine their impact on the model efficiency. Results indicated that the proposed model with monthly-variant RA is able to reproduce acceptable simulation results based on modified Kling-Gupta efficiency (KGE= -0.83). The results of density-based global sensitivity analysis for dry (June to September) and a wet (October to May) period reveal the dominant influence of RA (with sensitivity indices equal to 0.89 and 0.93, respectively) in spring discharge simulation. The sensitivity of simulated spring discharge to memory effect of different karst formations during the dry period is greater than the wet period. In addition, the results reveal the important role of intermediate-flow system in the hydrological modeling of karst systems during the wet period. Precise estimation of groundwater budgets for a better decision making regarding water supplies from complex karst systems with long memory effect can considerably be improved by use of the proposed model.

Key-Words: Groundwater Balance, Karst Memory, Conceptual Reservoir Model, Time-Variant Recharge Area, Global Sensitivity Analysis.

1. Introduction

Karst aquifers are of crucial importance for supplying drinking water worldwide (Ford and Williams 2007). A quarter of the world population is at least partially dependent on karst water resources (Stevanovic et al. 2016). 35% of Europe's land surface, which is more than 10% of the continental surface of our planet, consists of karst formations. Some European countries in the Mediterranean region are covered by karstified rocks of different lithology (for instance 25% of Spain, 33% of France and Turkey, and more than 40% of Slovenia and Croatia) and they rely on karst aquifers for 50% of their drinking water (Andreo et al. 2006; Lewin and Woodward, 2009). Karstic aquifers are characterized by a complex heterogeneous system created and developed by groundwater flows with great temporal and spatial hydrodynamic variability, caused by double or triple porosity structures, mixed flow nature,

and varying conduit permeability (Quinlan et al. 1996; Bakalowicz, 2005). These variations play an important role in the hydrograph profile of a karst spring (Doummar et al. 2012) and increase the difficulties in applying a verified model to another karst system (Anderson and Goulden 2011). For simulation of rainfall–runoff processes and analyzing of hydrological functioning in karst systems, conceptual models composed as a series of linear or nonlinear reservoirs are usually applied (e.g., Mangin 1975, Jukic and Denic-Jukic 2006, Fleury et al. 2007, Padilla and Pulido-Bosch 2008, Tritz et al. 2011, Hartmann et al. 2012, Zeljkovic and Kadic 2015). These studies consider one (Coutagne, 1968) or two main flow regimes as a function of the extent of aquifer karstification (Padilla et al. 1994; Stevanovic 2010; Kovacs et al. 2015): matrix-restrained flow regime (i.e. base-flow) and conduit-influenced flow regime (i.e. quick-flow) in the developed model structures. This leads to two segments for the falling limb of the spring hydrograph namely steep (or flood recession) and slightly sloped recession limb (or base-flow recession) and thus consideration of two distinct reservoirs of flows in the hydrological modeling of karst terrains. Nevertheless, besides the high-velocity flow through large dissolved fractures and diffuse flow in a diffusive network of smaller solutional openings, intermediate-flow can occur in well integrated karstified fissures as the result of a transient phenomenon in the vicinity of the high hydraulic conductivity channel network (Eienlohr et al., 1997). These three flow components can be clearly discriminated in a spring hydrograph by three successively distinctive slopes (Forkasiewicz and Paloc 1967; Baedke and Krothe, 2001; Kovacs and Perrochet 2008). The intermediate-flow in well-developed karst terrains plays a significant role during the high recharge periods. In these conditions, a strong pressure gradient exchanges flow between a conduit and diffuse continua (BacdKe and Krothe, 2001). Neglecting the intermediate-flow component or considering it as mixing of water moving through the conduits and the diffuse portions of rock matrix in the hydrological modeling of karst systems reduces the model accuracy and omits some details of

karst processes (Bonacci et al. 2006; Hosseini and Ataie-Ashtiani, 2017). Limited studies can be found that incorporate the intermediate-flow in the hydrological functioning of karst. Baedke and Krothe (2001) reported the significant contribution of the intermediate-flow system in spring hydrograph shape for two well-developed karst aquifers in Indiana by estimating the ratio of transmissivity and specific yield for three distinct karst flow systems. Long and Putnam (2004) analyzed time-series data of $\delta^{18}O$ in spring outlet and well in a karst aquifer to model the separate response and properties of traveling time of three flow components (conduit, intermediate, and diffuse) by integrating the linear-systems and mass balance approaches. While they considered three probability density functions as a transfer function in linear-system, the memory effect of conduits, intermediate, and diffuse flow systems for a karst aquifer in South Dakota were optimized as 8-14 days, 200-210 days, and 28 years, respectively. Butscher and Huggenberger (2008) developed four global models for simulating of karst spring discharge and assessing the vulnerability of the karst system. They incorporated recharge compartments from soil and epikarst system, intermediate-flow system, exchange flow between the conduit and the diffuse system and seasonal variation in the water storage capacity of the recharge system in the model structures.

Furthermore, the recharge area (RA) of a karst system can significantly vary over time (Goldscheider et al. 2007). The reservoir model is not able to reproduce groundwater balance calculations when an average RA is assumed. Even though varying RAs through the hydrological year have frequently been investigated in literature (e.g. Ravbar et al. 2012), only a few studies include them in their model structure. Hartmann et al. (2013) considered the variability of soil and epikarst depths to cope with spatial and temporal (yearly) variation of RA through a case study in southern Spain. They found that the RA changed significantly (from 28 to 53 km^2) in different hydrological years. Zeljkovic and Kadic (2015) developed a simple conceptual rainfall–runoff model considering two linear reservoirs for base-flow and

quick-flow systems to estimate the Opacac karst groundwater balance components in Croatia, while monthly-variant RA was considered during the hydrological year. Hosseini and Ataie-Ashtiani (2017) studied the dynamics of the transient interchange of water between conduits and diffusive networks in conditions of with/without surface recharge by linear-exchanged reservoirs model (i.e. dual-porosity approach) in a less developed karstic aquifer in Iran. The results indicated that considering constant RA during the hydrological year leads to the efficiency of both single porosity and dual-porosity models to be the same in the estimation of spring discharge during the recession period. Whereas dual-porosity model outperforms the single porosity during recharge period due to better representation of hydraulic properties of karst aquifer by introducing exchange flux of water between conduits and matrix. Alongside this challenge, knowledge of the memory of infiltrated water through different parts of karst aquifers is an invaluable tool for contaminant vulnerability assessment and evaluation of aquifer recharge rate during karst groundwater budget calculations and exploitation studies (Bailly-Comte et al. 2011). The term of memory effect of conduits, intermediate, and diffuse flow systems is assumed as the average groundwater travel time of the exchanged flow between the respective "reservoirs" to the point of observation in spring outlet (Stevanovic et al. 2016). The karst system memory, which also called aquifer inertia (Mangin 1981) or the response time of the karst system to input signal may be estimated by analyzing the cross correlation function (CCF) between the rainfall and spring discharge as time duration of the CCF function to reach the significant limit of 0.2 (Massei et al. 2006).

The CCF analysis also gives information about the quality of drainage, the groundwater reserves of the aquifer, identification of the main rainfall contribution, and the travel time through the main infiltration pathways in karst aquifers (Mangin and Pulido-Bosch 1983, Mayaud et al. 2014, Kavousi and Raeisi 2015). This technique usually results in a broad estimation of the time required for water to flow through an investigated karst aquifer ranging

from a few days to more than a year (Fiorillo et al. 2007, Fiorillo and Doglioni 2010). In modeling of karst hydrological functioning, there are some studies that considered the memory length of water recharged into groundwater less than the simulation time step which is usually considered one day (e.g., Zeljkovic and Kadic 2015). This leads to neglecting the memory effect of different karst formations (e.g. base-flow and quick-flow systems) to antecedent recharged flow. To the authors' knowledge, only, Jukic and Denic-Jukic (2006) developed a non-linear kernel function based on Volterra series whereas an antecedent recharge index (IAR) in exponential form is defined to consider the memory effect of the base-flow component and so, the shape of the kernel function. In complex karst systems, each component of base-flow, intermediate, and quick-flow are correlated to surface recharged flows in previous time steps depending on the degree of karstification, the thickness of soil cover, and the type of infiltration (Denic-Jukic and Jukic 2003).

Investigation of the temporal variation of RA on the water budget components during the hydrological year and also defining quantitative indices to incorporate the memory effect of different flow systems in karst hydrological modeling have not been systematically reported. Recently, Hosseini and Ataie-Ashtiani (2017) revealed the role of water exchange flux between two continua of conduits and matrix by comparison of two conceptual models, one considered single porosity and the other dual porosity approach. Following their study, the aim of this work is to develop a simple conceptual rainfall–runoff model for the estimation of groundwater balance components including the influences of intermediate flow storage, memory effect of different karst flow systems, and time-variant RA. The proposed model is divided into three sub-models to simulate the daily spring discharge: soil moisture balance (SMB), epikarst balance (EPB), and groundwater balance (GWB) as described in details in the following section. The SMB and EPB sub-models are expressed as the mass conservation equation to compute the variation of moisture storages in the soil cover and epikarst,

respectively. The GWB sub-model computes ordinates of discharge hydrograph through three parallel linear reservoirs for base-flow, intermediate, and quick-flows. Three antecedent recharge indexes are defined to deal with the dependency of these karst flow systems to the previous infiltrated water. In addition, the effect of invariable, two (winter and summer), four (seasonal), and monthly variation RA through the hydrological year are investigated on the efficiency of the proposed model. Finally, a density-based global sensitivity analysis has been carried out to assess the sensitivity of model output to the input parameters.

2. Materials and Methods

2.1. Model Development

The model used in this study for the estimation of groundwater balance is a modified lumped model similar to reservoirs models used in earlier works in karst systems (e.g. Rimmer and Hartmann, 2012, Zeljkovic and Kadic 2015). This model consists of three sub-models, shown in Figure 1, including 1) soil moisture balance model (SMB), 2) epikarst balance model (EPB), and 3) groundwater balance model (GWB) to obtain the complete form of karst aquifer budget. Two sub-models of SMB and EPB consider the hydrological functioning, storage and production of soil cover of karst formations and also epikarst components which have been applied and tested in karst aquifers. The modifications are conducted in the sub-model GWB by considering three parallel linear reservoirs to simulate base-flow (flow in the low-permeable matrix), intermediate-flow (well integrated karstified fissures), and quick-flow (flow in the conduit network) of total spring discharge which incorporates the memory length of each component to the input recharge separately in the sub-model structure.

It is assumed that the source of recharge to the upper karst formations is a direct infiltration from precipitation (autogenic recharge). The SMB model expresses the mass conservation equation between the variables of total precipitation on the karst surface P $[LT^{-1}]$, actual

evapotranspiration ET_a $[LT^{-1}]$, variation of moisture storages in the soil $dV_s/dt[LT^{-1}]$, and recharge to the underlying layers R_S $[LT^{-1}]$ during time step Δt (Zeljkovic and Kadic, 2015):

$$\frac{dV_S}{dt} = P(t) - ET_a(t) - R_S(t) \quad (1)$$

According to the Palmer (1965), the moisture loss from the soil cover is equal to ET_a $[LT^{-1}]$ which is function of precipitation P $[LT^{-1}]$, soil moisture storage V_S $[L]$, maximum capacity of soil to store the infiltrated water V_{ms} $[L]$, and potential evapotranspiration ET_P $[LT^{-1}]$ (Hartmann et al., 2015; Hosseini and Ataie-Ashtiani, 2017):

$$ET_a(t) = \begin{cases} ET_P(t) & if \quad V_s(t) + P(t) \times \Delta t \geq V_{ms} \\ ET_P(t) \times \dfrac{\frac{V_s(t)}{\Delta t} + P(t)}{\frac{V_{ms}}{\Delta t}} & if \quad V_s(t) + P(t) \times \Delta t < V_{ms} \end{cases} \quad (2)$$

The term of ET_P can be calculated from climatic data using the empirical methods such as Hargreaves-Samani (HS) equation (Hargreaves and Allen 2003), which provides a good estimation in arid and semi-arid regions of southern Iran and outperforms to other methods (Sepaskhah and Razzaghi 2009). The original form of HS equation is as follows:

$$ET_P = 0.408 \times KT \times (T_{mean} + 17.78) \times (T_{max} - T_{min})^{0.5} \times R_a \quad (3)$$

where ET_P is in mm day^{-1}, T_{max}, T_{min}, and T_{mean} are the mean daily maximum temperature, mean daily minimum temperature, and mean daily temperature in $^{\circ}$C, respectively; and R_a is the exteraterrestrial radiation (MJ m^{-2} day^{-1}). R_a depends on the Julian day number and the latitude of study area and can be computed as described by Allen et al. (1998). The coefficient of 0.408 is for converting MJ m^{-2} day^{-1} into mm day^{-1}, and KT is empirical coefficient which originally considered as 0.162 for interior regions (Hargreaves and Samani 1982)> Sepaskhah and Razzaghi (2009) modified the Hargreaves-Samani equation for semi-arid region of southern Iran as follows:

$$ET_P = 0.0026 \times (T_{mean} + 17.78) \times (T_{max} - T_{min})^{0.5} \times R_a \quad (4)$$

Equation (1) represents a linear differential equation (LDE) which can be solved numerically in each time step Δt with considering the maximum water storage in the soil layer as the initial value. Dependency of water stored at time t to precipitation and evapotranspiration in the previous times are related to thickness of soil cover, type of water infiltration (diffuse or concentrated) and also velocity of water through the soil layer (permeability). If the lag time of infiltrated water through the top soil is greater than the time step Δt, the equation (1) can be solved numerically using multi-step methods, such as Adams-Moulton method (AM) (Atkinson et al., 2009). For example, solving the equation (1) using a two-step AM method can be formulated as

$$\begin{cases} V_S(t) = V_S(t-\Delta t) + \frac{1}{2} \times \Delta t\big(f(t) + P(t-\Delta t) - ET_a(t-\Delta t) - R_S(t-\Delta t)\big) \\ f(t) = V_S(t-\Delta t) + \frac{3}{2} \times \Delta t\big(P(t-\Delta t) - ET_a(t-\Delta t) - R_S(t-\Delta t)\big) - \\ \qquad\qquad \frac{1}{2} \times \Delta t\left(P(t-2\Delta t) - ET_a(t-2\Delta t) - R_S(t-2\Delta t)\right) \end{cases} \quad (5)$$

Equation (5) means that the precipitations of two previous time steps are contribute to the water stored in the soil at the current time step. For aquifers with longer lag time, higher order AM method (e.g. fourth order) can be considered. When the lag time is smaller than Δt, equation (1) can be solved numerically using forward Euler's method as

$$V_S(t) = V_S(t-\Delta t) + [P(t-\Delta t) - ET_a(t-\Delta t) - R_S(t-\Delta t)] \times \Delta t \quad (6)$$

When the stored moisture in the soil layer reaches to its maximum capacity ($V_S(t) = V_{ms}$), the soil is saturated and the excess infiltrated water recharges to the epikarst as $R_S(t)[LT^{-1}]$. In the other word, the output of the SMB model is considered as the input of the EPB model (Figure 1-a). In the second sub-model, the variation of water stored in the epikarst $V_{epi}(t)[L]$ depends on the maximum capacity of epikarst to store water $V_{mepi}\,[L]$, moisture loss from epikarst production storage $L_{epi}(t)\,[LT^{-1}]$, and seepage or overflow from epikarst to underlying karst formations $R_{epi}(t)\,[LT^{-1}]$. Seepage from epikarst occurs when the water

stored in this part exceeds its maximum capacity (i.e. $V_{epi}(t) > V_{mepi}$) through the following mass balance equation:

$$\frac{dV_{epi}}{dt} = R_S(t) - L_{epi}(t) - R_{epi}(t) \quad (7)$$

The moisture loss from the epikarst production storage, $L_{epi}(t)$ can be considered as a function of saturation degree of this layer by the fraction of f_{epi} at time step Δt:

$$L_{epi}(t) = \frac{f_{epi} \times V_{epi}(t)}{\Delta t} \quad (8)$$

Similar to SMB sub-model, applying the two-step AM and forward Euler's methods for epikarst system with memory effect (i.e. the mean response time of infiltrated water into epikarst) greater and lower than Δt, respectively, the LDE of equation (5) can be solved numerically as follows:

$$\begin{cases} V_{epi}(t) = V_{epi}(t-\Delta t) + \frac{1}{2} \times \Delta t \left(g(t) + R_S(t-\Delta t) - L_{epi}(t-\Delta t) - R_{epi}(t-\Delta t) \right) \\ g(t) = V_{epi}(t-\Delta t) + \frac{3}{2} \times \Delta t \left(R_S(t-\Delta t) - L_{epi}(t-\Delta t) - R_{epi}(t-\Delta t) \right) - \\ \qquad \frac{1}{2} \times \Delta t \left(R_S(t-2\Delta t) - L_{epi}(t-2\Delta t) - R_{epi}(t-2\Delta t) \right) \end{cases} \quad (9)$$

$$V_{epi}(t) = V_{epi}(t-\Delta t) + \left[R_S(t-\Delta t) - L_{epi}(t-\Delta t) - R_{epi}(t-\Delta t) \right] \times \Delta t \quad (10)$$

After epikarst balance model, the seepage or overflow from epikarst, i.e. $R_{epi}(t)$ which is also considered as the effective precipitation to groundwater (P_{eff}) is the input for third sub-model or groundwater balance model (GWB). The sub-model of GWB transforms the effective precipitation (P_{eff}) to discharge hydrograph through exchanging flow between three parallel linear reservoirs. The recharge to underlying karst formations by the $P_{eff}(t)$ or $R_{epi}(t)$ is divided into the low-permeable network of pores and narrow fissures as base-flow, intermediate system of well-integrated karstified fissures as intermediate-flow, and conduit network as quick-flow, respectively through three separation factors f_b, f_{im} and f_q (which

$f_b + f_{im} + f_q = 1$). The base-flow reservoir has a long response time and recession after rainy season, whereas the quick-flow reservoir shows rapid infiltration during rainfall events. Each reservoir of base-flow, intermediate-flow, and quick-flow transforms its groundwater storage $V_b\,[L], V_{im}\,[L]$, and $V_q\,[L]$ to exchangeable discharge $q_b[LT^{-1}], q_{im}[LT^{-1}]$ and $q_q[LT^{-1}]$ between the reservoirs through the corresponding reservoir constants of $K_b\,[T]$, $K_{im}\,[T]$, and $K_q\,[T]$:

$$q_b = \frac{V_b}{K_b} \quad , \quad q_{im} = \frac{V_{im}}{K_{im}} \quad , \quad q_b = \frac{V_q}{K_q} \tag{11}$$

where the constants of $K_b\,[T]$, $K_{im}\,[T]$, and $K_q\,[T]$ are the drainage speed of each reservoirs and define as reciprocal to recession coefficients of $\alpha_b\,[T^{-1}]$, $\alpha_{im}\,[T^{-1}]$, and $\alpha_q\,[T^{-1}]$ respectively. Changes in the reservoir storages V_b, V_{im}, and V_q can be related to their input recharge and discharge by continuity equation (Singh, 1988) using following LDEs:

$$\frac{dV_b}{dt} = f_b \times P_{eff}(t) - q_b \rightarrow \frac{dq_b}{\alpha_b dt} = f_b \times P_{eff}(t) - q_b \tag{12-1}$$

$$\frac{dV_{im}}{dt} = f_{im} \times P_{eff}(t) - q_{im} \rightarrow \frac{dq_{im}}{\alpha_{im} dt} = f_{im} \times P_{eff}(t) - q_{im} \tag{12-2}$$

$$\frac{dV_b}{dt} = f_b \times P_{eff}(t) - q_b \rightarrow \frac{dq_b}{\alpha_q dt} = f_b \times P_{eff}(t) - q_b \tag{12-3}$$

Using the analytical solution of above LDEs and applying the initial conditions ($t = 0, q = q_0$) provide the following specific solutions for estimation of ordinates of discharge from different karst formations $Q_b\,[L^3T^{-1}]$, $Q_{im}[L^3T^{-1}]$, and $Q_q\,[L^3T^{-1}]$:

$$Q_b(t) = Q_b(t - \Delta t) \times e^{-\alpha_b t} + \frac{f_b \times P_{eff}(t) \times A(t)}{\Delta t} \times (1 - e^{-\alpha_b t}) \tag{13-1}$$

$$Q_{im}(t) = Q_{im}(t - \Delta t) \times e^{-\alpha_{im} t} + \frac{f_{im} \times P_{eff}(t) \times A(t)}{\Delta t} \times (1 - e^{-\alpha_{im} t}) \tag{13-2}$$

$$Q_q(t) = Q_q(t - \Delta t) \times e^{-\alpha_q t} + \frac{f_q \times P_{eff}(t) \times A(t)}{\Delta t} \times (1 - e^{-\alpha_q t}) \tag{13-3}$$

$$Q_{spring}(t) = Q_b(t) + Q_{im}(t) + Q_q(t) \tag{13-4}$$

where $Q_{spring}(t)[LT^{-3}]$ is the total discharge of karst system in each time step t, q_{0b}, q_{0im}, and q_{0q} are discharges at the beginning of recession curves of three components; $A(t)[L^2]$ is effective RA of karst aquifer with time variations (Figure 1-b). The concept of "effective recharge area" in this study denotes to the area of conduits network, the intermediate system of fractures, and the fissures matrix that contribute to spring discharge through exchanging water between the corresponding reservoirs. Since the conduits networks and intermediate system of fractures are embedded within the fissure matrix, the variations of area of these components during time were taken into account by $A(t)$. Whereas the proposed model considered the variation in recharge area connected to spring outlet, the catchment boundaries (i.e. surface recharge area) was assumed constant during the hydrological year. Based on this assumption, the areas of infiltrated water through the top soil and also epikarst are constant during the hydrological year and equal to the catchment area. The influences of time-variant catchment boundaries are considered in the previous studies in daily scale (Hartmann et al. 2013) or monthly scale (Jukic and Denic-Jukic 2009) as calibration parameters. Considering daily variant RA in the equation (13) will dramatically increase the model dimensions and therefore run time and computation cost of the model. In this study, the influences of monthly ($A(t), t$=1, 2,…, 12), seasonally ($A(t), t$=1, 2, 3, 4), two ($A(t), t$=1, 2), and invariable RA are investigated in terms of the efficiency of the proposed model. Discretizing the RA in time allows this variable to be treated as time-independent during each interval and also to account for the internal changes of groundwater level in that time period. Moreover, it gives a better representation of characteristics of the karst spring functioning during the hydrological year and increases the applicability of the water balance equation (Jukic and Denic-Jukic 2009).

Equations (13-1) to (13-4) are valid under the assumption that the response time (or memory length) of water infiltrated into groundwater is less than the time step Δt (which is usually 1 day). However, different parts of a karst system including conduit network, intermediate

system, and low permeable fissures indicate a wide range of water pore pressure transfer times (e.g. Fiorillo et al., 2009). This leads to the discharge components of Q_b, Q_{im}, and Q_q being connected to the antecedent cumulative recharged flows. To incorporate the impact of memory effect of flow in low permeable fissures, intermediate system of well integrated karstified fissures, and conduit network parts, three indices of antecedent recharges, $IAR_b\ [L], IAR_{im}\ [L]$and $IAR_q\ [L]$ are defined:

$$IAR_b(i) = \sum_{j_1=0}^{\min(i,l_b)} P_{eff}(i-j_1) \qquad (14-1)$$

$$IAR_{im}(i) = \sum_{j_2=0}^{\min(i,l_{im})} P_{eff}(i-j_2) \qquad (14-2)$$

$$IAR_q(i) = \sum_{j_3=0}^{\min(i,l_q)} P_{eff}(i-j_3) \qquad (14-3)$$

where $l_b\ [-]$, $l_{im}\ [-]$, and $l_q[-]$ are dependency length of the base-flow, intermediate-flow, and quick-flow in the current time step to the antecedent recharges (i.e. memory length). It is evident that due to variability of permeability in different parts of karst system, $l_q < l_{im} < l_b$. Jukic and Denic-Jukic (2006) approximated the memory effect and dependency length of the quick-flow component to the aquifer recharge with the exponential function of Maillet (1905) in a nonlinear kernel function to develop instantaneous unit hydrograph of a bare Dinaric karst aquifer in Croatia.

Finally, the modified form of equation (13) to estimate the i^{th} ordinates of spring discharge is as follows:

$$Q_{spring}(i) = Q_b(t-1) \times\ e^{-\alpha_b t} + \frac{f_b \times A(t)}{\Delta t} \times (1 - e^{-\alpha_b t}) \times IAR_b(i) +$$

$$Q_{im}(t-1) \times\ e^{-\alpha_{im} t} + \frac{f_{im} \times A(t)}{\Delta t} \times (1 - e^{-\alpha_{im} t}) \times IAR_{im}(i) +$$

$$Q_q(t-1) \times e^{-\alpha_q t} + \frac{f_q \times A(t)}{\Delta t} \times (1 - e^{-\alpha_q t}) \times IAR_q(i) \quad (15)$$

With time step being 1 day. It should be mentioned that under the conditions of ignoring intermediate-flow component (i.e. second part in R.H.S of equation 14), and non-dependency of base-flow and quick-flow components to the antecedent recharges ($l_q = l_b$=1), the equation (15) will reduce to one developed by the Jukic and Denic-Jukic (2006), Rimmer and Hartmann (2012), Hartmann et al. (2013), and Zeljkovic and Kadic (2015) and Hosseini and Ataie-Ashtiani (2017).

2.2. Model Calibration

The model inputs are time series of daily rainfall (P), daily actual evapotranspiration (ET_a), and also recession coefficients of three flow components $\alpha_b, \alpha_{im}, \alpha_q$. The corresponding model output is simulated ordinates of daily spring discharge (Q_{spring}). Parameters of the model are adjusted during the calibration phase. A summary of all model parameters and their range for the calibration according to previous studies (e.g. Hartmann et al. 2013; Zeljkovic and Kadic 2015; Hosseini and Ataie-Ashtiani 2017) are listed in Table (1). Considering the monthly variation of effective RA (A), the developed model has 21 parameter for adjustment (V_{ms}, V_{mepi}, f_{epi}, f_b, f_{im}, f_q, l_b, l_{im}, l_q and 12 parameters for $A(t)$). The parameters of the proposed model reduced to 10 when a constant RA is considered throughout the hydrological year. Three recession coefficients of α_b, α_{im}, and α_q can be directly estimated from the decomposition of base-flow, intermediate-flow, and quick-flow recession curves according to Forkasiewicz and Paloc (1967) and Kovacs and Perrochet (2008). The parameter ranges of l_b, l_{im}, and l_q can be estimated by CCF between time series of observed base-flow, intermediate-flow, and quick-flow ordinates with cumulative precipitation P data. Since the estimation of P_{eff} depends on the parameters which need to be calibrated, thus linear cross-

correlation function (CCF), $r_{QP}(k)$ between the discharge ordinates with cumulative P data (up to 365 days) and also autocorrelation function (ACF) of spring discharge ($r_{QQ}(k)$) are used for estimation of initial range of these parameters (Fiorillo and Doglioni 2010):

$$r_{QP}(k) = \frac{COV\ (Q,P)}{S_Q \times S_P} \tag{16}$$

where $COV\ (Q,P)$ is the covariance between the spring discharge time series Q, and the rainfall time series P, computed at time lag k. S_Q and S_P are the standard deviations of the time series. CCF function between P and Q practically indicates asymmetric shape around the origin (i.e. k=0). In such condition, cross-spectral function (CSF) presents remarkable information for the duration of different flow components (i.e. memory effect) and how the karst system attenuates the input signal (i.e. P) in different frequencies (Biddiscombe et al. 1985). In this regard, the cross-gain function (G_{PQ}) gives notable results (Padilla and Pulido-Bosch 1995):

$$G_{PQ}(f) = \frac{\alpha_{PQ}(f)}{\sqrt{\Gamma_P(f)}} \tag{17}$$

where $\alpha_{PQ}(f)$ is cross-amplitude between series of P and Q for the frequency f (i.e. f=1/period (day)), and $\Gamma_P(f)$ is spectral density function of the series P for the frequency f. According to Padilla and Pulido-Bosch (1995) and Laroque et al. (1998), the f values (or periods) correspond to G_{PQ}=1 and 0.4 are equivalent to the frequencies (or durations) of base-flow and quick-flow compartments.

It should be mentioned that the CCF and G_{PQ} give an initial estimation for the range of mean travel time of flow through the main infiltration pathways in three karst flow systems (i.e. summation of l_b, l_{im}, and l_q) which need to adjusted during the calibration mode. For calibration of the proposed model, the modified Kling-Gupta efficiency KGE (Gupta et al.,

2009) is used as objective (fitness) function of the optimization problem to adjust the parameters

$$KGE = \sqrt{(r-1)^2 + (\gamma-1)^2 + (\beta-1)^2} - 1 \quad , \quad \gamma = \frac{Q_s^{sim}}{Q_s^{obs}}, \quad \beta = \frac{Q_m^{sim}}{Q_m^{obs}} \tag{18}$$

where r is the correlation coefficient between simulations and observations ordinates of spring discharge, Q_s^{sim}, Q_s^{obs} and Q_m^{sim}, Q_m^{obs} are the standard deviations and means of simulated and observed ordinates of discharge, respectively. The ratios of γ and β represents the variability and the bias term, respectively. The fitness function of KGE needs to be minimized with an ideal value at -1. KGE is identified as a strong performance criterion for calibration of hydrological models (Wohling et al., 2013). A genetic algorithm (GA) with real coding (Goldberg, 1989) is implemented to determine optimal sets of the parameters (so called decision variables) of the developed model with minimizing KGE as the fitness function and the range of parameters given in Table (1) as the constraints. All computations needed for model development are programmed in MATLAB environment (Release #14). A warm-up period of three years of initial data is considered for the calibration phase to reduce the effects of initial values of the parameters on the model performance.

2.3. Global Sensitivity Analysis of the Proposed Model

Density based sensitivity indices (DSI) have become progressively widespread in Global Sensitivity Analysis (GSA) applications across different hydrological modeling fields (e.g. Liu et al. 2006, Pappenberger et al. 2008, Peeters et al. 2014, Rajabi et al. 2015). In the DSI approach proposed by the Pianosi and Wagener (2015) which named PAWN, the model output distribution is characterized by data sample Cumulative Distribution Function (CDF) rather than its PDF. Practically in the PAWN indices, the sensitivity to input x_i is measured by the distance between the empirical unconditional CDF of output y, $\hat{F}_y(y)$ that is obtained

when all inputs vary simultaneously, and the empirical conditional CDF, $\hat{F}_{y|x_i}(y)$ that are obtained when varying all inputs but x_i is fixed at a nominal value, through the Kolmogorov-Smirnov statistic, $\widehat{KS}$ (Kolmogorov 1933):

$$\widehat{KS}\,(x_i) = \max_{y} \left|\hat{F}_y(y) - \hat{F}_{y|x_i}(y)\right| \tag{19}$$

The empirical unconditional CDF of variable y, $\hat{F}_y(y)$ is approximated using N_u output estimations obtained by sampling the entire input feasibility region. The conditional CDF y, $\hat{F}_{y|x_i}(y)$ is approximated using N_c output estimations obtained by sampling the non-fixed inputs only, while the value of x_i is held fixed. As statistics KS depends on the value at which x_i is fixed, the index $\hat{T}_i$ considers the maximum values of $\widehat{KS}$ over all possible values of x_i (Saltelli et al. 2008):

$$\hat{T}_i = \max_{\mathrm{x_i} = \bar{\mathrm{x}}_\mathrm{i}^{(1)}, \bar{\mathrm{x}}_\mathrm{i}^{(2)}, \ldots, \bar{\mathrm{x}}_\mathrm{i}^{(\mathrm{n})}} \left|\widehat{KS}(x_i)\right| \tag{20}$$

where $\bar{\mathrm{x}}_\mathrm{i}^{(1)}, \bar{\mathrm{x}}_\mathrm{i}^{(2)}, \ldots, \bar{\mathrm{x}}_\mathrm{i}^{(\mathrm{n})}$ are randomly sampled values for the fixed input x_i. The lower value of $\hat{T}_i$, ($\hat{T}_i \in [0,1]$) indicates the lower influence of the corresponding x_i on y. The total number of model evaluations necessary to compute the sensitivity indices $\hat{T}_i$ for all the N_{param} inputs is $N_u + n \times N_c \times N_{param}$. The proper values for n, N_u and N_c can be selected by trial-and-error to follow regularity properties of CDFs (continuity, monotonicity, relative smoothness). The indices $\hat{T}_i$ is global, model independent, robust, quantitative, dimensionless, with no need for parameter tuning, no computing costs for computing the CDF, easy to implement and facilitates the application of bootstrapping and convergence analysis, and is unconditional on any assumed input value (Pianosi et al. 2015). In this study, the sensitivity index ($\hat{T}_i$) of the daily spring discharge (Q_{spring}) to ten input parameters V_{ms}, V_{mepi}, f_{epi}, f_b, f_{im}, f_q, l_b, l_{im}, l_q and A are calculated using Eqs. (19) and (20) for two dry (June to September) and wet

seasons (October to May), separately. The index $\hat{T}_i$ is helpful tool to investigate the relative influence of model parameters over the predictive accuracy to support model calibration and simplification, as well to understand the dominant factors which control the model precision.

3. Study Area and Data Sets

The performance of the developed model is studied in the karstic Sasan aquifer located at the Kazeroun region in south-west of Iran, 51˚ 35' E longitude, 29˚ 47' N latitude (Figure 2). Sasan spring is the biggest karstic spring of this region which emerged from the Dashtak aquifer at an elevation of 814 m a.s.l.. This spring is the main water supply of the cities of Kazeroun and Bushehr located on the coast of the Persian Gulf. The famous and popular location for tourist visits is Shapour cave and it is located in the catchment area of this spring. Geologically the study area is a part of Simply Folded Zagros zone which consists of long, linear, asymmetrical folds in which anticlines are well exposed and separated by broad valleys (Miliaresis 2001).

Dye-tracing studies revealed that the RAs of these springs are located in adjacent anticlines and reach the Dashtak anticline via its northwestern plunge apex (Milanović and Aghili 1993, Karst Research Center of Iran, 2002) as shown in Figure (2). The Shapour River traverses the Dashtak anticline near the north-eastern plunge apex, developing a deep valley, namely the Chugan Valley, resulting in the flow of this river over the impervious Pabdeh-Gurpi Formations and acts as a local base level. Therefore, hydraulic connectivity of the Asmari-Jahrum Formations (consists of limestone and dolomite) with a thickness of 1000 m in the northern and southern limbs and is disrupted by the high elevation of the Pabdeh-Gurpi Formations (consists of marl and shale) with a thickness of 1140 m beneath the crest of the anticline, except in the northwestern plunge apex area (Ashjari and Raeisi 2006) (Figure 2). Sasan Spring emerges near the end of the Chugan Valley, a few meters above the Shapour

River water level. Stratigraphic columns in the study area are well described in Alavi (2004) and McQuarrie (2004).

The hydrogeological characteristics of the karstic aquifer have been formed during a long evolutionary process, as a consequence of very dynamic new tectonic activity in the Zagros geotectonic unit (Milanović and Aghili, 1993). Based on a previous study (Hosseini and Ataie-Ashtiani, 2017) the karst system of the studied aquifer has a deep phreatic zone, partly or totally confined underneath impermeable sediments, and largely karstified during previous karstification phases.

According to Figure (3-a), the mean daily discharge of Sasan spring is 2.26 m^3/s (71.3 million cubic meters per year). In the catchment of the springs, precipitation is the only recharge source for this karstic aquifer. The mean annual precipitation (MAP) recorded by the meteorological station in the Kazeroun is 597.5 mm, whereas the maximum and minimum precipitation occur in January (143.7 mm) and June (0.65 mm) respectively. The maximum and minimum monthly discharges recorded in the outlet of springs are 3.93 m^3/s (in March) and 1.41 m^3/s (in October). The spatial heterogeneity of the precipitation (P) and actual evapotranspiration (ET_a) over the surface RA was neglected due to lack of local weather stations. Therefore, these variables have been considered as lumped through the catchment area.

Continuous long-term daily meteorological data (1985 to 2012) were available from a meteorological station in the catchment (Qaemieh station), and corresponding daily discharge data for the spring outlet were given from the Iranian Water Resources Management Company (Figure 4). No gap was observed in these data, but time series of P and Q data indicate a significant decreasing trend due to climate change after 1998 as shown in Figure (3-b).

At the spring outlet, a limnigraph (water-level recorder) records the water level values and daily discharge data is obtained through the scale-discharge relationship. Recession curves of three springs indicate successive exponential decreasing limbs with various slopes suggesting that karst systems of each aquifer consist of multiple reservoirs, all contributing to the discharge of the spring. Time series analysis of daily rainfall (P) and discharge (Q) (Figure 4) shows that on average a lag time of 43 days (between 6-85 days) is observed between the time of maximum precipitation and maximum discharge. These lag times may be considered as the earliest estimation of the memory effect of whole karst formations (including top soil, epikarst, and systems of fast, intermediate, and base flow) to the surface recharge. Fifteen recession curves (thick curves in Figure 4) are used and decomposed to estimate the three recession coefficients of α_b, α_{im}, and α_q.

The catchment area of Sasan spring is previously determined through the following equation (Bonacci et al. 2006) and verified by some tracer tests by Ashjari and Raeisi (2006):

$$CA = \frac{V}{1000 \times P \times I_C} \tag{21}$$

where CA is the average annual hydrological catchment area of the spring (km^2), V is the total annual discharge of the spring during hydrological year (m^3), P is the annual precipitation (mm yr^{-1}), and I_C is average annual effective infiltration coefficients ($0 < I_C < 1$). Equation (21) is valid in conditions of no allogeneic stream input and the variation of storage over time is insignificant. Ashjari and Raeisi (2006) estimated the recharge coefficient I_C as 0.37 which results in a hydrological catchment area of 332 km^2.

4. Results and Discussions

4.1. Cross Correlation Analysis of Rainfall and Discharge Data

To estimate the memory length of karst flow systems, analysis of CCF and CSF between the spring discharge with precipitation data on the catchment ($r_{QP}(k)$) and autocorrelation of

spring discharge ($r_{QQ}(k)$) are computed and the obtained results are shown in Figure (5). The slow decrease of the autocorrelation coefficient, $r_{QQ}(k)$, suggests that there are high memory effects (up to 90 days) in this karst system which is in the ranges of lag times data between the time of maximum precipitation and maximum discharge shown in Figure (3).

The cross-correlation function (CCF) of Figure (5-a) has a mild slope and shows two peaks where the first occurs with a lag of 18 days (related to fast flow component) and the second with a lag of 58 days (related to base flow component). The evidence of existing different flow components could be seen in the gain function of Figure (5-b), as a strong attenuation of correlations occurs in the frequencies less than 0.015 and 0.04 (equivalent to periods 67 and 25 days). The coefficients of function G_{PQ} can be considered insignificant for frequencies greater than 0.25 (periods less than 4 days) which indicates the karst system remarkably attenuates the infiltrated P series for such frequencies. The frequencies corresponding to values G_{PQ}=1 and 0.4 are 0.016 and 0.05, respectively. These values respectively indicate the durations of base-flow and quick-flow in the karst aquifer according to Padilla and Pulido-Bosch (1995). The intermediate-flow has a frequency between 0.016 to 0.05.

The significant dependency of long time intervals of rainfall appears to be the main component affecting the spring hydrograph, i.e. base-flow, whereas short time intervals are related to quick-flow. This dynamic behavior of the karst system was also reported by Fiorillo and Doglioni (2010) for Caposele and Torano kart springs in southern Italy and by Stevanovic et al. (2016) for six karst springs in south eastern Dinarides, Slovenia. These analyses contributed to providing an overview of the time required for infiltrated rainfall to the flow through the karst aquifer.

4.2. Analysis of Recession Curves

Three recession coefficients of α_b, α_{im}, and α_q are obtained from the decomposition of base-flow, intermediate-flow, and quick-flow recession curves and entered directly into the model structure for calibration and validation phases of corresponding periods. For this purpose, 15 identified recession curves from observed spring data for the period 1986-2005 are used and the results are summarized in Table (2). Average recession period is 274 days which is characteristic of a slow draining aquifer. This is a long period in comparison to some other studies (e.g. Padilla et al. 1994, Fiorillo and Doglioni 2010) but they are similar to ones reported by El-Hakim and Bakalowicz (2007) for Zarka karst systems in Lebanon. Average value of recession curves, α_b, α_{im}, and α_q are obtained 0.0033 day^{-1}, 0.031 day^{-1}, and 0.181 day^{-1}, respectively based on analysis of 15 recession curves. These values lead to reservoir storage 303.0 days, 32.3 days, and 5.5 days, respectively for slow, intermediate, and quick-flow systems. The storage constants for the slow and quick systems were smaller than other studies such as; Hartmann et al. (2012) but are similar to Fleury et al. (2009), Geyer et al. (2008), Rimmer and Salingar (2006), and Zeljkovic and Kadic (2015). High storage volumes and very slow system dynamics of the base-flow are most probably explains why the spring never fell dry.

4.3. Calibration and Validation of the Proposed Model

Using the available daily rainfall, temperature, and spring discharge data from 1985 to 2005 and using the KGE (Equation 16) as the objective function, the proposed model is calibrated using the genetic algorithm (GA) in a predefined, physically plausible calibration range considering previous studies (as listed in Table 1). The proposed model is calibrated and validated under four scenarios of time-variant RA as invariable, two (winter and summer), four (seasonal), and twelve (monthly) through the hydrological year. The first three years of data are used as a warm up period to account for uncertainties in initial conditions. The

numbers of generations required for the GA to converge are obtained 52, 136, 470, and 477 (by averaging the three times of algorithm run) respectively for invariable, two (winter and summer), four (seasonal), and twelve (monthly) RA scenarios. In the four cases, the GA settings including population size, crossover rate, and mutation probability are considered to be 20, 0.8, and 0.1, respectively. The proposed model with monthly RA achieves minimum KGE value at the end of calibration period (-0.83), while invariable RA leads to KGE=-0.52. This indicates a better fit of the monthly-variant model to estimate the spring discharge (the optimum value of KGE is -1).

The results of parameter adjustments of the proposed model considering the temporal variation of RA through the hydrological year are given in Table (3). As seen in this Table, considering the RA to groundwater as time-variant parameter in the proposed model structures affected the adjusted values of the other parameters. This shows that the RA to groundwater (i.e. area of exchange flow between three components of base, intermediate, and quick-flows) affected the dynamic behavior of all karst formations. The values of f_{epi} indicate that the losses from stored water in epikarst is between 23% to 35%. Most of the recharged water to the groundwater (P_{eff} or R_{epi}) directed to the base-flow system with separation factor f_b equal to 0.41 to 0.51, which indicated very slow system dynamics and high storage volumes of the study aquifer. In the previous work (Hosseini and Ataie-Ashtiani, 2017), a value of 0.28 is obtained for separation factor of conduit network of this aquifer by using dual-porosity (including only base-flow and quick-flow) model. Zeljkovic and Kadic (2015) reported the base-flow separation factor between 0.55 to 0.61 for Opacac karst spring in Croatia; Hartmann et al. (2013) calibrated the recharge fraction to conduit system as 0.63 for a karst spring in Southern Spain; and Hartmann et al. (2012) obtained a base-flow separation factor 0.06 for Faria spring, Eastern Mediterranean. The memory length of base-flow system (l_b) is optimized between 59 days (for monthly variation RA scenario) to 73

days (for invariable RA scenario). The minimum memory effect adjusted for the quick-flow system between 11 to 18 days. The average values of memory length for base, intermediate and quick-flow systems (l_b, l_{im}, and l_q) to the recharged water from upper layer are optimized with averages of 63, 27, and 15 days for different scenarios for RAs. The calibrated values of memory lengths for quick and base flow systems when monthly variation RA scenario assumed in the proposed model coincide with the times correspond to the peaks observed in CCF analysis (Figure 5-a), and also frequencies 0.016 and 0.05 correspond to the G_{PQ}=1 and 0.4, respectively in the cross-spectral analysis (Figure 5-b).

The model adjusted RA is equal to 261.8 km^2 for constant RA condition, whereas values of 326.5 km^2 and 175.0 km^2 are obtained for the winter and summer, respectively. For the case of seasonal RA, maximum and minimum RAs are equal to 151.2 km^2 and 344.2 km^2 which are close to values obtained using the double RA condition. For the monthly RA condition, the maximum area is obtained for March and is equal to 352.3 km^2 with a two month delay related to the time for maximum precipitation to occur (i.e. January). Whereas the minimum RA is obtained for September and is equal to 125.2 km^2. Interestingly, the average RA obtained for time-variant catchment boundaries (226 km^2) are less than that adjusted for other RA scenarios (which are close together between 250-261 km^2) and all are greater than ones obtained by classical and dual-porosity (i.e. 174 and 185 km^2, respectively) models reported in the previous work (Hosseini and Ataie-Ashtiani 2017) and close to those obtained by tracer studies (Ashjari and Raeisi 2006). This difference is possibly due to precise the calculation of water balance components (e.g. ET_a estimation method) and better quantification of the hydraulic properties of karst dynamic behavior through the present model. Specifically, the proposed model with monthly RA provides a better representation of the internal changes in groundwater level when considering the variations of exchange

surface area of three reservoirs corresponding to the fast, intermediate, and base-flow systems during hydrological year.

4.4. Validation of the Proposed Model

Using the adjusted model parameters in four scenarios of constant, double, seasonal, and monthly variation RA (Table 3), the efficiency of the proposed model is validated for the period of 1997-2005 (Figure 6). A good fit is observed between the simulated and observed hydrographs for time-variant RA (i.e. monthly), whereas the simulated hydrograph obtained by considering the constant RA during hydrological year indicates the largest deviation from the observed hydrograph (Figure 6-b). Three goodness of fit criteria including root mean squares of error ($RMSE$), correlation coefficient (R^2), and KGE between the results of proposed model with different RA scenarios and corresponding observed values are computed and given in Figure (6-c). The maximum and minimum KGE values for validation period of the proposed model are obtained for monthly RA (-0.71) and constant RA (-0.39), respectively. The average root mean square of error ($RMSE$) of 1.25 and 1.66 is obtained between the observed mean annual discharge and estimated corresponding values by the proposed model with monthly-variation and constant RA, respectively. The results indicate that considering the temporal variation of RA (or catchment boundaries) during the hydrological year, leads to more reliability of the proposed model in simulation of discharge and also water balance components based on criteria of KGE, R^2 and $RMSE$ (Figure 6-c). To investigate the effect of time-variation RA on water balance components, the average values of Et_a, V_s, R_s, V_{epi}, L_{eppi}, and P_{eff} estimated by the proposed model for two conditions of constant and monthly-variant RA during the validation period are shown in Figure (7). The maximum discrepancies between two cases (constant and monthly-variant RA) are on average related to the recharge to underlying karst formations, P_{eff} (199.6 and

217.8 *mm/year*, respectively), the water storage in soil, V_s (161.3 and 153.2 *mm/year*, respectively), and followed by the epikarst, V_{epi} (243.0 and 232.1 *mm/year*, respectively). The minimum variability between constant and monthly-variant RA is observed for the component L_{epi} (75.1 and 72.4 *mm/year*, respectively).

4.5. Results of Density-based Global Sensitivity Analysis

The conditional, $\hat{F}_y(y)$ and unconditional, $\hat{F}_{y|x_i}(y)$ cumulative density function (CDF) of the proposed model output (Q_{spring}) for 10 input parameters of V_{ms}, V_{mepi}, f_{epi}, f_b, f_{im}, f_q, l_b, l_{im}, l_q, and A are computed (the results are not shown). The CDFs of all parameters grow significantly away from their initial uniform distributions. If a parameter is sensitive, it would differ significantly from a uniform distribution. Using this criterion, the model output Q_{spring} is sensitive to the parameter A, followed by V_{ms}, and f_q. The model output is less sensitive to the parameter f_{epi}, which means that it could adapt to a wide range of values without changing the simulation results (Q_{spring}). These findings are consistent with those reported by Hartmann et al. (2015) and Hartmann et al. (2012) which indicated that the VarKarst model output has the maximum and minimum sensitivity to the parameter A and V_{epi}, respectively.

The maximum distance between the conditional and unconditional CDFs of model output, Q_{spring} to the input parameter ($\widehat{KS}$ statistic) are computed using the Equation (19) and the obtained result shows in Figure (8). In this figure, the critical values of KS statistic at a confidence level of 0.05 are also shown (dashed red lines). The values below the critical value indicate the $\widehat{KS}$ statistic is non-significant for its parameter value. The maximum $\widehat{KS}$ statistic is obtained for the RA (A) especially for small values of this parameter. This reveals the significant influence of RA during the recession period. Previously, Hartmann et al.

(2015) demonstrated the importance of yearly-variant catchment area in hydrological karst modeling by developing VarKarst model. For the parameters f_{epi} and V_{mepi}, all values of the $\widehat{KS}$ are less than its critical values. This suggests the proposed model is not sensitive to the moisture loss from the epikarst production storage and the maximum storage water in soil portion. The model is sensitive to the parameter capacity of soil (V_{ms}) but only for the small values of this parameter. This means that the model is not influenced by the bare karst formations or small thickness of top soil and epikarst. For karst systems with deep soil surface, the model is not sensitive to soil moisture capacity. The model is influenced by the base and intermediate-flow systems when the karst systems are not karstified (low values of these parameters) or highly karstified aquifers (high values of these parameters). The effect of a quick-flow system is significant only for high values of f_q (i.e. highly karstified aquifers). The spring discharge is more affected by the lower memory length of the intermediate-flow system. The proposed model is sensitive to the formations with low (karstified conduit aquifers) and high memory length of base-flow system (less karstified aquifers). These findings are consistent with those reported by Hartmann et al. (2015) and Hartmann et al. (2012) which indicated that the VarKarst model output has the maximum and minimum sensitivity to the parameter A and V_{epi}, respectively.

According to Equation (20), the sensitivity index $\hat{T}_i$ is considered as the maximum values of $\widehat{KS}$ over all possible values of each input parameter. This index can be useful for ranking the sensitivity of model output (Q_{spring}) to the input parameters. For more comparisons, the sensitivity index of the spring discharge to the input parameters ($\hat{T}_i$) has been assessed for two periods of dry (June to September) and wet (October to May), separately (Figure 9). Results of GSA for the assumed model and used data sets indicated that the most influential parameters on the spring discharge for both dry and wet periods are RA (A) followed by intermediate flow storage (f_{im}) and then soil capacity (V_{ms}). Greater value of $\hat{T}_i$ for RA

during dry period (i.e. 0.88) indicates the effect of exchange flow-area variability between three components of base, intermediate, and quick-flow systems under conditions of no surface recharge. The effect of soil capacity (V_{ms}) and intermediate-flow (f_{im}) on the spring discharge are significantly different in the wet and dry periods where the infiltrated and deep recharge flow is significant. Whereas the effect of other parameters has not a significant difference in both wet and dry periods. But the parameters f_{epi} and V_{mepi} exert minimum influence on simulation of spring discharge for both dry and wet periods. The values of $\widehat{KS}$ over all possible values of these parameters are statistically non-significant (Figure 9). Other parameters (e.g. f_b, f_q, l_b, l_{im}, and l_q) have the same influence on the spring discharge for both dry and wet periods. This leads to the loss of epikarst production that can be eliminated in the proposed model structure.

Over-parametrization of the proposed model especially when the RA is considered in monthly scale (including 21 parameters) is an issue that needs to be discussed. The principle of parsimony (Box and Jenkins 1976) suggests the structure of the selected hydrological model should be reduced to only components that describe the key process of the system. However, an over-parameterized model probably would be faced with challenges in model implementation, calibration and parameter adjusting, uncertainty analysis, and interpretation of their results, but a parsimonious model do not necessary guarantee that all the hydrological processes of the complex karst system are represented (Kuczera and Mroczkowski 1998, Sellami et al. 2014). Removing less-sensitive parameter (based on GSA), applying the appropriate calibration procedure (i.e. two-step), and reducing the dimension of the parameters space based on field evidence are approaches to reduce parameter uncertainties, saving time and cost of computation for parameter adjustment, and also increasing the accuracy of high dimensional models.

5. Conclusion

In this study, we have developed a simple conceptual rainfall–runoff model for the estimation of groundwater balance components in complex karst system, including three sub-models SMB, EPB, and GWB. In the proposed model, three parameters have been considered to deal with the influences of memory length of base-flow, intermediate-flow, and quick-flow systems. In addition, the effect of time-variant catchment boundaries (constant, six-monthly, seasonal, and monthly) is also assessed to simulate the daily spring discharge by the developed model. Results indicated that the proposed model with monthly-variant RA showed an adequate agreement with daily spring discharge and also water balance components (especially for V_s P_{eff}) in a case study in the south-west of Iran. However, the model with monthly-variant catchment boundaries leads to over-parameterization (with 21 parameters) when comparing to other cases, but the density-based GSA indicated that the RA is the most influential parameter in the model structure for both dry (absence of surface recharge) and wet (existence of surface recharge) periods. After the RA, intermediate-flow and the water stored in the top soil layer (for the wet period), and quick-flow and memory effect of different components (for the dry period) play important roles in groundwater balance.

Our study showed that when conceptualizing hydrological functioning of a complex karst system with reservoir models, the intermediate-flow system due to transient phenomena that occurs in the vicinity of the high conductivity channels. The results of GSA also indicated that the intermediate-flow storage in karst system plays an influential role of these parameters especially when large volumes of recharged water pass through this system (i.e. during the wet period). Whereas the parameter of moisture loss from epikarst and maximum capacity of soil and epikarst to store water can be omitted from the model structure since the related sensitivity indices are insignificant.

Our analysis also indicated that incorporating the memory length of base-flow, intermediate-flow, and quick-flow systems to the antecedent recharged flows seems to be an effective compartment in the model setup for the simulation of spring discharge ordinates.

It should be noted that since each karst system has its individual characteristics, the features included in the proposed model are examples of possible important processes that can improve the modeling results, whereas other field sites may require the presence of different processes in the model structure. The results obtained are valid for the assumed model structure and for the data set used in the study area, whereas another model structure would probably lead to other conclusions. Nevertheless, depending on the developed model to the low data is of its great advantage. Incorporating mass balance approach in the model setup limits the model efficiency for the predictions especially in circumstances different from those that have been observed. Neglecting of spatial heterogeneity of some influenced variables (e.g. precipitation, actual evapotranspiration, and thickness of soil and epikarst) over the RA is another simplification in the proposed model which may affect the reliability of the obtained results (e.g. overestimation of the catchment area).

Finally, combining the linear reservoirs approach in addition to the water balance equation provides a detailed and better representation of the hydrology of complex karst systems with long memory and thick top soil. It is an effective tool for karst groundwater balance estimation and supports decision making for karst water management.

Acknowledgements

The authors appreciate the constructive comments of the Editor-in-Chief Dr. Geoff Syme and anonymous reviewers that helped to improve the final version this paper. The authors Behzad Ataie-Ashtiani and Craig T. Simmons acknowledge support from the National Centre for Groundwater Research and Training, Australia.

Nomenclatures

A.S.L	Above sea level
A $[L^2]$	Effective recharge area of karst aquifer
$COV\ (Q,P)$	Covariance between the Q and P time series
ET_P $[LT^{-1}]$	Potential evapotranspiration
ET_a $[LT^{-1}]$	Actual evapotranspiration
f_b $[-]$	Separation factor of base-flow
f_{epi} $[-]$	Fraction of moisture loss from the epikarst
f_{im} $[-]$	Separation factor of intermediate-flow
f_q $[-]$	Separation factor of quick-flow
$\hat{F}_y(y)$	Empirical unconditional CDF of y
$\hat{F}_{y\|x_i}(y)$	Empirical conditional CDF of y
IAR_b $[L]$	Indices of base-flow antecedent recharge
IAR_{im} $[L]$	Indices of intermediate-flow antecedent recharge
IAR_q $[L]$	Indices of quick-flow antecedent recharge
$\widehat{KS}$	Kolmogorov-Smirnov statistic
KGE $[-]$	Modified Kling-Gupta efficiency
K_b $[T]$	Reservoir constants of base-flow
K_{im} $[T]$	Reservoir constants of intermediate-flow
K_q $[T]$	Reservoir constants of quick-flow
l_b $[-]$	Memory length of base-flow in karst system
l_{im} $[-]$	Memory length of intermediate-flow in karst system
l_q $[-]$	Memory length of quick-flow in karst system

L_{epi} $[LT^{-1}]$	Loss from epikarst storage
P $[LT^{-1}]$	Total precipitation on the karst surface
P_{eff} $[LT^{-1}]$	Effective precipitation to groundwater
q_b $[LT^{-1}]$	Specific base-flow discharge
q_{im} $[LT^{-1}]$	Specific intermediate-flow discharge
q_q $[LT^{-1}]$	Specific quick-flow discharge
$\bar{Q}$ $[L^3T^{-1}]$	Average spring discharge
Q_b $[L^3T^{-1}]$	Base-flow discharge
Q_{im} $[L^3T^{-1}]$	Intermediate-flow discharge
Q_q $[L^3T^{-1}]$	Quick-flow discharge
Q_{spring} $[L^3T^{-1}]$	Spring discharge
r_{QP} $[-]$	Cross-correlation function between the discharge and precipitation
r_{QQ} $[-]$	Autocorrelation function of spring discharge data
R_S $[LT^{-1}]$	Recharge to the karst formation
R_{epi} $[LT^{-1}]$	Seepage from epikarst to underlying karst formations
S_P $[L]$	Standard deviations of the precipitation time series
S_Q $[L^3T^{-1}]$	Standard deviations of the discharge time series
$\hat{T}_i$ [-]	Maximum values of $\widehat{KS}$
V_b $[L]$	Volume of base-flow storage
V_{epi} $[L]$	Water stored in the epikarst
V_{im} $[L]$	Volume of intermediate-flow storage
V_{mepi} $[L]$	Maximum capacity of epikarst to store water
V_{ms} $[L]$	Maximum capacity of soil storage
V_q $[L]$	Volume of quick-flow storage

$V_s\ [L]$	Soil moisture storage
$\beta\ [-]$	Bias of simulated discharge data
$\gamma\ [-]$	Variability of simulated discharge data

6. References

Alavi, M., 2004. Regional stratigraphy of the Zagros Fold–Thrust Belt of Iran and its proforeland evolution. American Journal of Science, 304, 1–20.

Allen, R.G., Pereira, L.S., Raes, D., and Smith, M. 1998. Crop evapotranspiration: Guidelines for computing crop requirements. Irrigation and Drainage Paper No. 56, FAO, Rome, Italy.

Anderson, R.G., and Goulden, M.L., 2011. Relationships between climate, vegetation, and energy exchange across a montane gradient. J. Geophys Res. 116(G1), G01026, 1-16. DOI:10.1029/2010jg001476.

Ashjari, J., and Raeisi, E. 2006. Influence of anticlinal structure on regional flow, Zagros, Iran. Journal of Cave and Karst Studies, 68(3), 118−129.

Atkinson, K., Han W., and Stewart D., 2009. Numerical solution of ordinary differential equations. John Wiley & Sons, Inc., Hoboken, New Jersey. Published simultaneously in Canada, pp 261.

Baedke, S.J., and Krothe, N.C., 2001. Derivation of effective hydraulic parameters of a karst aquifer from discharge hydrograph analysis. Water Resources Research 37(1), 13-19.

Bailly-Comte, V., Martin, J.B., and Screaton, E.J., 2011. Time variant cross correlation to assess residence time of water and implication for hydraulics of a sink-rise karst system, Water Resour. Res. 47, W05547. DOI 10.1029/2010WR009613.

Bakalowicz, M., 2005. Karst groundwater: a challenge for new resources. Hydrogeology Journal 13(1), 148–160.

Biddiscombe, E.F., Rogers, A.L., Allison, H. and Litchfield, R., 1985. Response of groundwater levels to rainfall and to leaf growth of farm plantations near salt seeps. Journal of Hydrology 78, 19-34.

Bonacci, O., Jukic, D., and Ljubenkov, I. 2006. Definition of catchment area in karst: case of the rivers Krčić and Krka, Croatia, Hydrological Sciences Journal 51(4), 682-699. DOI: 10.1623/hysj.51.4.682

Bonacci, O., Ljubenkov, I., and Roje-Bonacci, T., 2006. Karst flash floods: an example from the Dinaric karst (Croatia) Nat. Hazards Earth Syst. Sci. 6, 195–203.

Box, G.E.P, and Jenkins, G.M., 1976. Time series analysis: Forecasting and control. Rev. ed. San Francisco. Holden-Day.

Butscher, C., and Huggenberger, P., 2008. Intrinsic vulnerability assessment in karst areas: A numerical modeling approach, Water Resour. Res., 44, W03408, DOI 10.1029/2007WR006277.

Denic-Jukic, V., and Jukic, D., 2003. Composite transfer functions for karst aquifers. Journal of Hydrology 274(1-4), 80-94.

Doummar, J., Sauter, M., and Geyer, T., 2012. Simulation of flow processes in a large scale karst system with an integrated catchment model (Mike She)—identification of relevant parameters influencing spring discharge. Journal of Hydrology 426,112–123.

Eisenlohr, L., Kiraly, L., Bouzelboudjen, M., and Rossier, Y., 1997. Numerical simulation as a tool for checking the interpretation of karst spring hydrographs. Journal of Hydrology 193, 306-315.

El-Hakim, M., and Bakalowicz, M., 2007. Significance and origin of very large regulating power of some karst aquifers in the Middle East. Implication on karst aquifer classification. Journal of Hydrology 333, 329– 339.

Fiorillo, F., 2009. Spring hydrographs as indicators of droughts in a karst environment. Journal of Hydrology 373, 290–301

Fiorillo, F., and Doglioni, A., 2010. The relation between karst spring discharge and rainfall by cross-correlation analysis (Campania, southern Italy). Hydrogeology Journal 18, 1881–1895.

Fiorillo, F., Esposito, L., and Guadagno, F.M., 2007. Analyses and forecast of water resources in an ultra-centenarian spring discharge series from Serino (southern Italy). Journal of Hydrology 336, 125–138.

Fleury, P., Ladouche, B., Conroux, Y., Jourde, H., Doerfliger, N., 2009. Modelling the hydrologic functions of a karst aquifer under active water management – the Lez spring. Journal of Hydrology 365(3–4), 235–243.

Fleury, P., Plagnes, V., and Bakalowicz, M., 2007. Modelling of the functioning of karst aquifers with a reservoir model: Application to Fontaine de Vaucluse (South of France). Journal of Hydrology 345, 38– 49

Ford, D.C., and Williams, P.W., 2007. Karst hydrogeology and geomorphology. Chichester: Wiley.

Forkasiewicz, J., and Paloc, H., 1967. Le regime de tarissement de la Foux de la Vis. Etude preliminaire. AIHS Col. Hydrol. Des roches fissures, Dubrovnik (Yugoslavia), 1, 213-228.

Geyer, T., Birk, S., Liedl, R., and Sauter, M., 2008. Quantification of temporal distribution of recharge in karst systems from spring hydrographs. J. Hydrol. 348, 452–463.

Goldscheider, N., and Drew, D., 2007. In: Hydrogeologists, I.A.o. (Ed.), Methods in Karst Hydrogeology. Taylor & Francis Group, p. 264, ISBN: 978-0-415-42873-6.

Gupta, H.V., Kling, H. Yilmaz, K.K., and Martinez, G.F., 2009. Decomposition of the mean squared error and NSE performance criteria: Implications for improving hydrological modelling, Journal of Hydrology 377, 80–91.

Hargreaves, G.H., and Allen, R.G. 2003. History and Evaluation of Hargreaves Evapotranspiration Equation. Journal of Irrigation and Drainage Engineering, 129(1), 53-63.

Hargreaves, G.H., and Samani, Z.A. 1982. Estimation of potential evapotranspiration. Journal of Irrigation and Drainage Division, Proceedings of the American Society of Civil Engineers 108, 223-230.

Hartmann, A., Barbera, J.A., Lange, J., Andreo, B., and Weiler, M., 2013. Progress in the hydrologic simulation of time variant recharge areas of karst systems – Exemplified at a karst spring in Southern Spain. Advances in Water Resources 54, 149–160.

Hartmann, A., Gleeson, T., Rosolem, R., Pianosi, F., Wada, Y., and Wagener, T., 2015. A large-scale simulation model to assess karstic groundwater recharge over Europe and the Mediterranean. Geosci. Model Dev. 8, 1729–1746.

Hartmann, A., Lange, J., Vivo Aguado, A., Mizyed, N., Smiatek, G., and Kunstmann, H., 2012. A multi-model approach for improved simulations of future water availability at a large Eastern Mediterranean karst spring. Journal of Hydrology 468–469, 130–138.

Hosseini, S.M., and Ataie-Ashtiani, B., 2017. Conceptualization of Karstic Aquifer with Multiple Spring Outlets by Dual Porosity Reservoir Model. Groundwater. DOI: 10.1111/gwat.12504

Hosseini, S.M., Mahjouri, N., and Bagheri, S., 2014. Monthly karstic spring flow forecasting using a sequential gaussian simulation technique Environ Earth Sci 72(9), 3531-3548. DOI10.1007/s12665-014-3262-1.

Jukic, D., and Denic-Jukic V., 2006. Nonlinear kernel functions for karst aquifers. J Hydrol. 328, 360–374.

Jukic, D., and Denic-Jukic V., 2009. Groundwater balance estimation in karst by using a conceptual rainfall–runoff model. J Hydrol. 373, 302–315.

Karst Research Centre of Iran, 1993. Comprehensive study and research in water resource of the Maharlu Basin, Fars: Karst Research Centre of Iran Report, v. 1–4.

Karst Research Centre of Iran. 2002. Result of dye tracing test in catchment area of Sasan Spring: Karst Research Centre of Iran Report, 91 p.

Kavousi, A., and Raeisi, E., 2015. Estimation of groundwater mean residence time in unconfined karst aquifers using recession curves. Journal of Cave and Karst Studies 77(2), 108–119. DOI: 10.4311/2014ES0106

Kolmogorov, A., 1933. Sulla determinazione empirica di una legge di distribuzione. G. Ist. Ital. Attuari 4, 83-91.

Kovács, A., and Perrochet, P., 2008. A quantitative approach to spring hydrograph decomposition. Journal of hydrology 352 (1), 16-29.

Kovács, A., Perrochet, P., Darabos, E., and Szűcs, P., 2015. Well hydrograph analysis for the characterisation of flow dynamics and conduit network geometry in a karst aquifer, Bükk Mountains, Hungary. Journal of Hydrology 530, 484-499.

Kuczera, G., and Mroczkowski, M., 1998. Assessment of hydrologic parameter uncertainty and the worth of multiresponse data. Water Resources Research 34(6), 1481-1489.

Larocque, M., Mangin, A., Razack, M., and Banton, O., 1998. Contribution of correlation and spectral analyses to regional study of a large karst aquifer (Charentes, France) J. Hydrol. 205(3–4), 217–231.

Liu, H., Sudjianto, A., and Chen, W., 2006. Relative entropy based method for probabilistic sensitivity analysis in engineering design. J. Mech. Des. 128, 326-336.

Long, A.J., and Putnam, L.D., 2004. Linear model describing three components of flow in karst aquifers using ^{18}O data. Journal of Hydrology, 296, 254–270.

Maillet, E., 1905. Essais d'hydraulique Souterraine et Fluviale. Hermann, Paris, p. 218.

Mangin, A., 1975. Contribution a` l'e´tude hydrodynamique des aquife`res karstiques. 3e`me partie. Constitution et fonctionnement des aquife`res karstiques. Annales de Spe´le´ologie 30 (1), 21–124.

Masseia, N., Dupont, J.P., Mahler, B.J. , Laignel, B. , Fournier, M. , Valdes, D., and Ogier, S. 2006. Investigating transport properties and turbidity dynamics of a karst aquifer using correlation, spectral, and wavelet analyses. Journal of Hydrology 329(1–2), 244–257.

Mayaud, C., Wagner, T., Benischke, R., and Birk, S., 2014. Single event time series anayseis in a binary karst catchment evaluated using a groundwater model (Lurbach system, Austria). J Hydrol 511, 628–639.

McQuarrie, N., 2004. Crustal scale geometry of the Zagros Fold–Thrust Belt, Iran. Journal of Structural Geology 26, 519–535.

Milanović, C., and Aghili, B., 1993. Hydrogeological characteristics and groundwater mismanagement of Kazerun karstic aquifer, Zagros, Iran, in Proceedings, Intern. Symposium on Hydrogeological Processes in Karst Terrenes, Antalya, Turkey, October 1990, IAHS publication, No. 207: Wallingford, IAHS Press, p. 163–171.

Miliaresis, G., 2001. Geomorphometric Mapping of Zagros Ranges at Regional Scale Computers & Geosciences 27, 775-786.

Padilla, A., and Pulido-Bosch A., 1995. Study of hydrographs of karstic aquifers by means of correlation and cross-spectral analysis. Journal of Hydrology 168, 73-89.

Padilla, A., and Pulido-Bosch, A., 1995. Study of hydrographs of karstic aquifers by means of correlation and cross-spectral analysis. Journal of Hydrology 168 (1), 73-89.

Padilla, A., and Pulido-Bosch, A., 2008. Simple procedure to simulate karstic aquifers. Hydrological Process 22(12),1876–1884.

Padilla, A., Pulido-Bosch, A., and Mangin, A., 1994. Relative Importance of Base-flow and Quickflow from Hydrographs of Karst Spring, Ground Water 32, 267–277.

Palmer, W.C., 1965. Meteorological drought, US Department of Commerce, Research Paper No. 45, Washington DC, 58 p.

Pappenberger, F., Beven, K., Ratto, M., and Matgen, P., 2008. Multi-method global sensitivity analysis of flood inundation models. Adv.Water Resour. 31 (1), 1-14.

Peeters, L.J.M., Podger, G.M., Smith, T., Pickett, T., Bark, R.H., and Cuddy, S.M., 2014. Robust global sensitivity analysis of a river management model to assess nonlinear and interaction effects. Hydrol. Earth Syst. Sci. 18(9), 3777–3785.

Perrin, C., Michel, C., and Andreassian, V., 2001. Does a large number of parameters enhance model performance? Comparative assessment of common catchment model structures on 429 catchments, J. Hydrol., 241, 275–301.

Pianosi, F., and Wagener, T., 2015. A simple and efficient method for global sensitivity analysis based on cumulative distribution functions. Environmental Modelling & Software 67, 1-11.

Pianosi, F., Sarrazin, F., and Wagener, T., 2015. A Matlab toolbox for Global Sensitivity Analysis (Short communication). Environmental Modelling & Software 70, 80-85

Quinlan, J.F., Davies, G.J., Jones, S.W., and Huntoon, P.W., 1996. The application of numerical models to adequately characterize ground-water flow in karstic and other triple-porosity aquifers. In: Ritchy JD, Rumbaugh JO (eds) Subsurface fluid-flow modeling, ASTM STP 1288. American Society for Testing and Materials (ASTM), West Conshohocken, pp 114–133.

Rajabi, M., Ataie-Ashtiani, B., and Janssen, H., 2015. Efficiency enhancement of optimized Latin hypercube sampling strategies: Application to Monte Carlo uncertainty analysis and meta-modeling. Advances in Water Resources 76, 127-139.

Ravbar, N., Barberá J.A., Petric, M., Kogovsek, and Andreo, J.B., 2012. Study of hydrodynamic behaviour of a complex karst system under low-flow conditions using natural and artificial racers (springs of the Unica River, SW Slovenia). Environmental Earth Sciences 65(8), 2259–2272.

Rimmer, A., and Hartmann, A., 2012. Simplified conceptual structures and analytical solutions for groundwater discharge using reservoir equations. In: Nayak, D.P.C. (Ed.), Water Resources Management and Modeling. InTech, Kakinada, India, ISBN: 978-953-51-0246-5.

Rimmer, A., and Salingar, Y., 2006. Modelling precipitation-streamflow processes in karst bassin: the case of the Jordan River sources, Israel. Journal of Hydrology 331 (3–4), 524–542.

Saltelli, A., Ratto, M., Andres, T., Campolongo, F., Cariboni, J., Gatelli, D., Saisana, M., Tarantola, S., 2008. Global Sensitivity Analysis, The Primer. Wiley.

Sellami H., La Jeunesse I., Benabdallah, S., Baghdadi, N., and Vanclooster, M., 2014. Uncertainty analysis in model parameters regionalization: a case study involving the SWAT model in Mediterranean catchments (Southern France). Hydrol. Earth Syst. Sci. 18, 2393–2413. DOI 10.5194/hess-18-2393-2014

Sepaskhah, A.R., and Razzaghi, F.H. 2009. Evaluation of the adjusted Thornthwaite and Hargreaves-Samani methods for estimation of daily evapotranspiration in a semiarid region of Iran. Archives of Agronomy and Soil Science 55 (1), 51- 6.

Singh, V.P., 1988. Rainfall–runoff modelling, hydrologic systems, Vol 1 and 2. Prentice-Hall, Englewood Cliffs.

Stevanovic, Z., 2010. Utilization and regulation of springs.- In: Kresic, N. & Z. Stevanovic (eds.). Groundwater hydrology of springs: Engineering, theory, management and sustainability. Elsevier, pp. 341-389, Amsterdam.

Stevanović, Z., Krešić, N., and Kukurić, N., 2016. Karst without Boundaries. CRC Press, Taylor and Francis Group, London, UK, 365 pp.

Tritz, S., Guinot, V., and Jourde, H., 2011. Modelling the behaviour of a karst system catchment using non-linear hysteretic conceptual model. Journal of Hydrology 397(3–4), 250–262.

Wohling, T., Samaniego, L., and Kumar, R., 2013. Evaluating multiple performance criteria to calibrate the distributed hydrological model of the upper Neckar catchment. Environ Earth Sci, 69, 453–468. DOI 10.1007/s12665-013-2306-2

Zeljkovic, I. and Kadic, A., 2015. Groundwater balance estimation in karst by using simple conceptual rainfall–runoff model. Environ Earth Sci. 74, 6001–6015. DOI 10.1007/s12665-015-4624-z

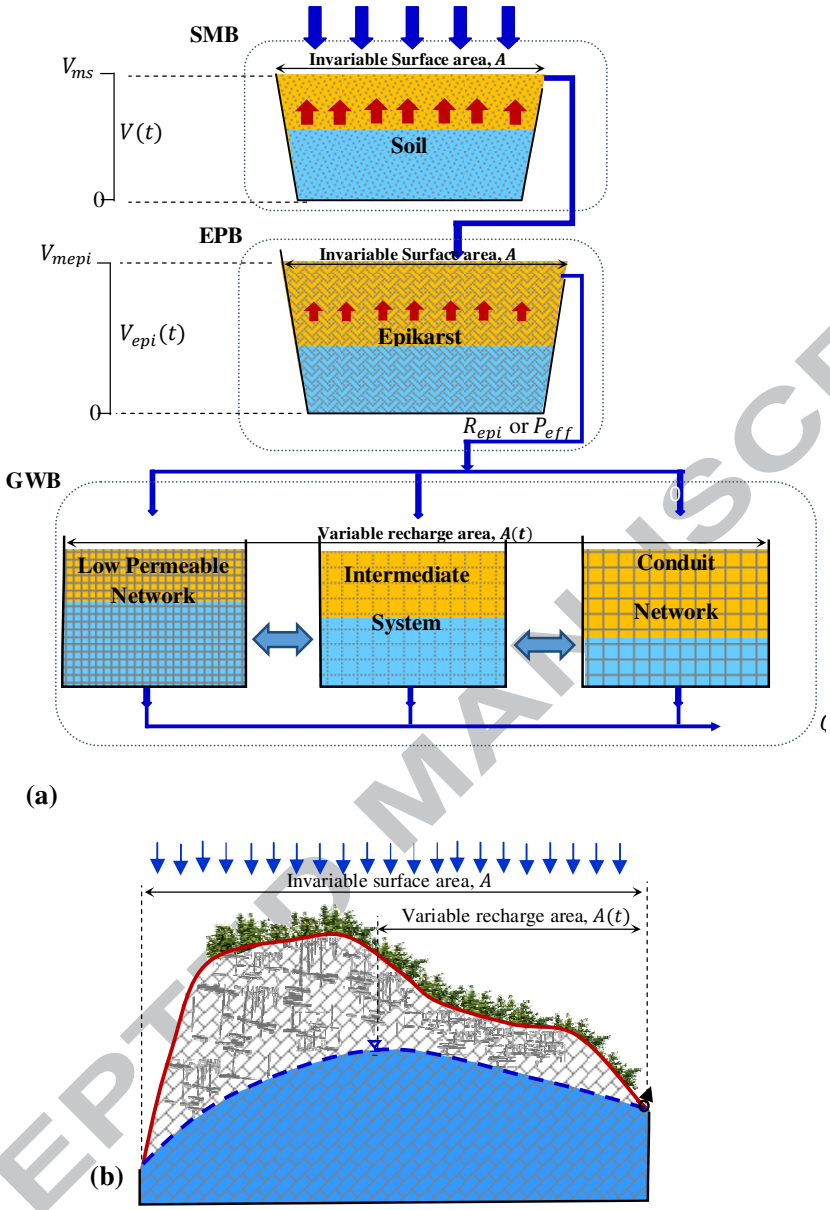

Figure (1): Sketch of conceptual model structure proposed for the groundwater balance estimation in karst aquifer (a), and concept of time-variant recharge area to spring outlet in the GWB sub-model (b).

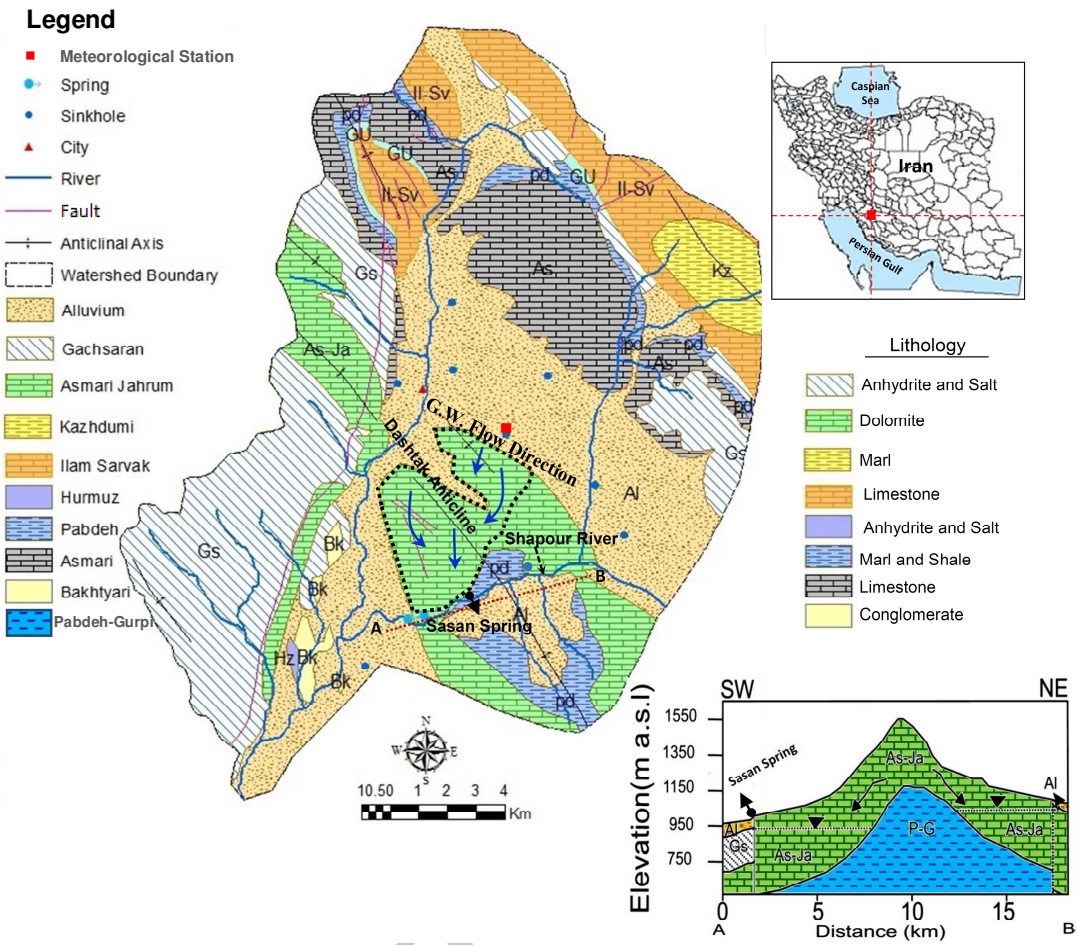

Figure (2): Hydrogeologic map and regional groundwater flow and geologic cross sections of Sasan karstic aquifer (Hosseini and Ataie-Ashtiani, 2016).

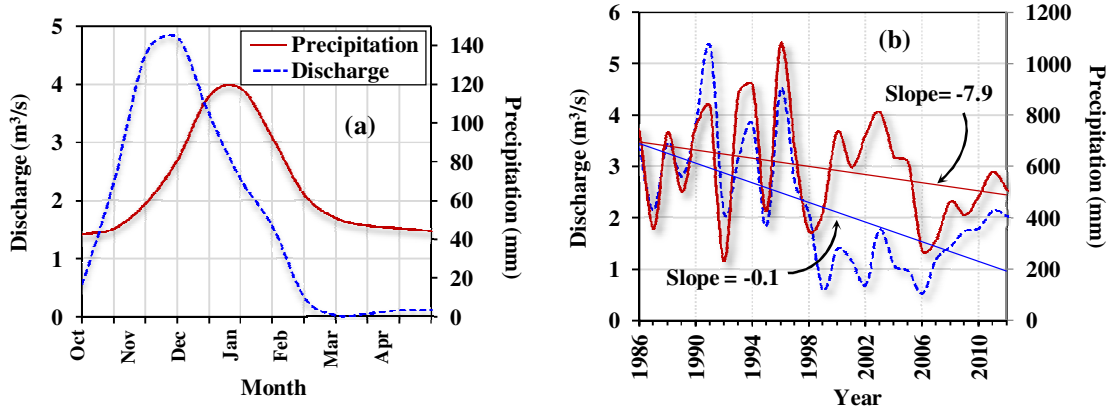

Figure (3): Monthly average of spring discharge and rainfall over the spring catchment (a) and long-term trends of mean annual precipitation and discharge data for Sasan spring (b).

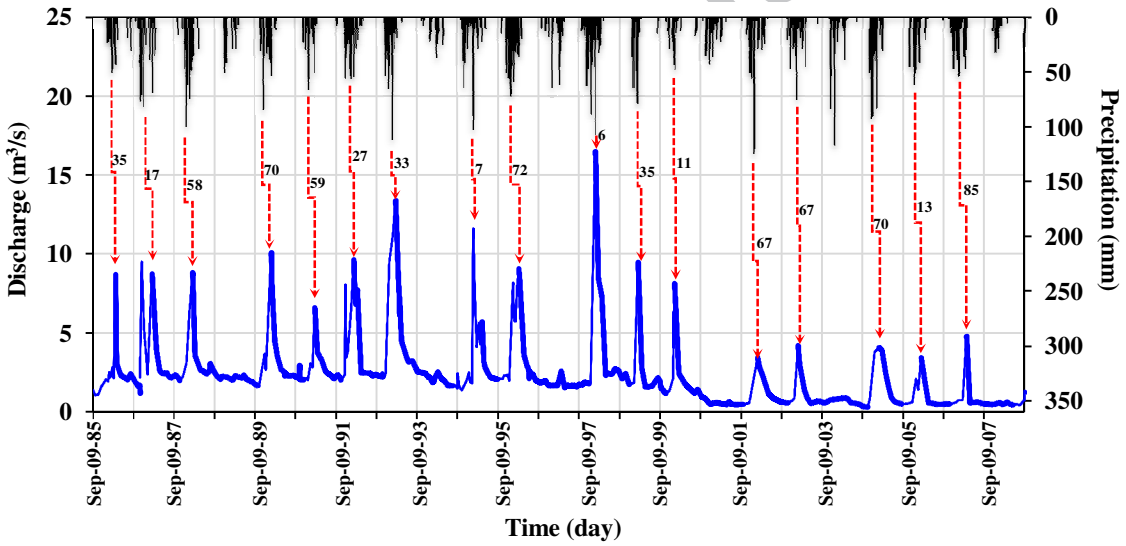

Figure (4): Time series of daily spring outlet and rainfall over the spring catchment. Thick lines along the graph are recession curves which are considered for calculating the coefficients of α_b, α_{im}, and α_q. Numbers on the figure indicate the lag time (day) between the time of maximum precipitation and maximum discharge in each year.

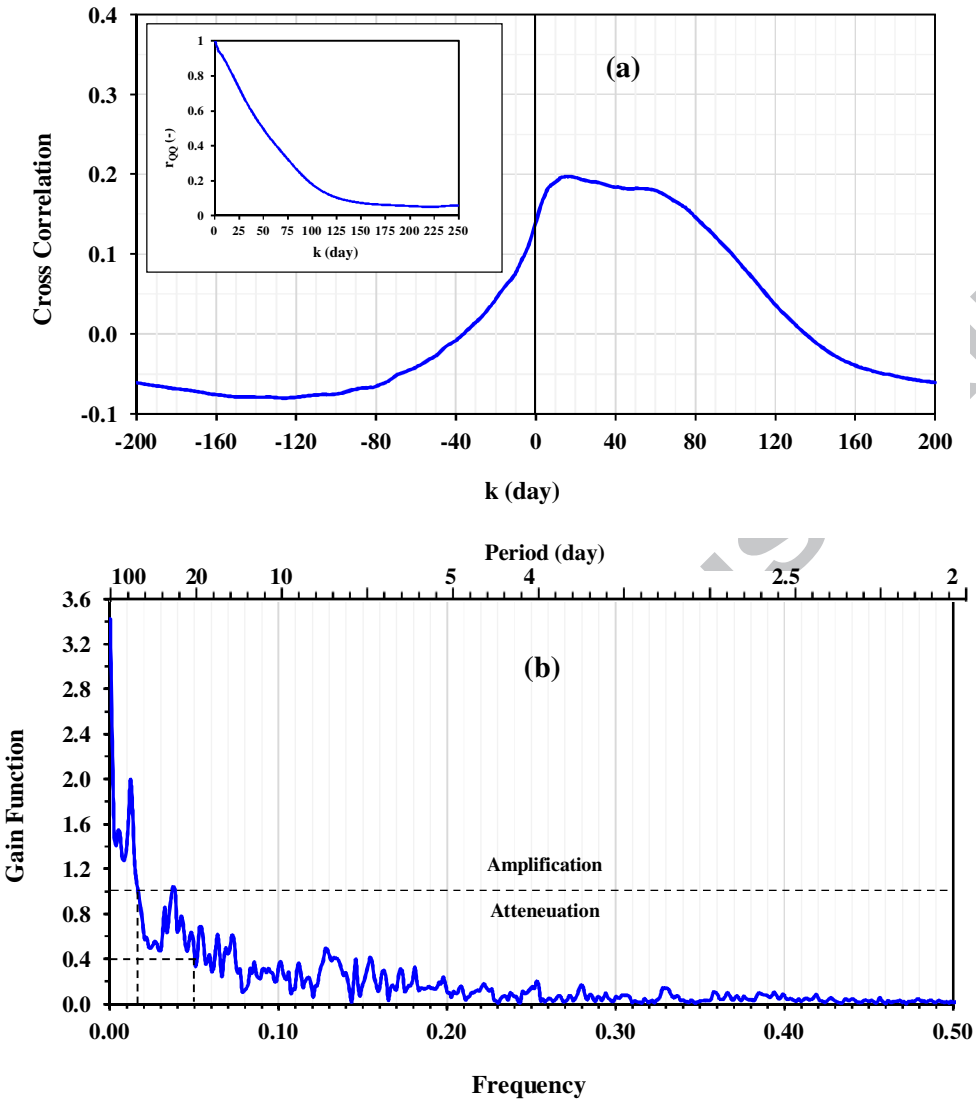

Figure (5): Cross-correlation function between daily precipitation and discharge ($r_{QP}(k)$), and ACF of spring discharge ($r_{QQ}(k)$) (a), and gain function for series of P and Q obtained in cross-spectral analysis (b) for the study aquifer.

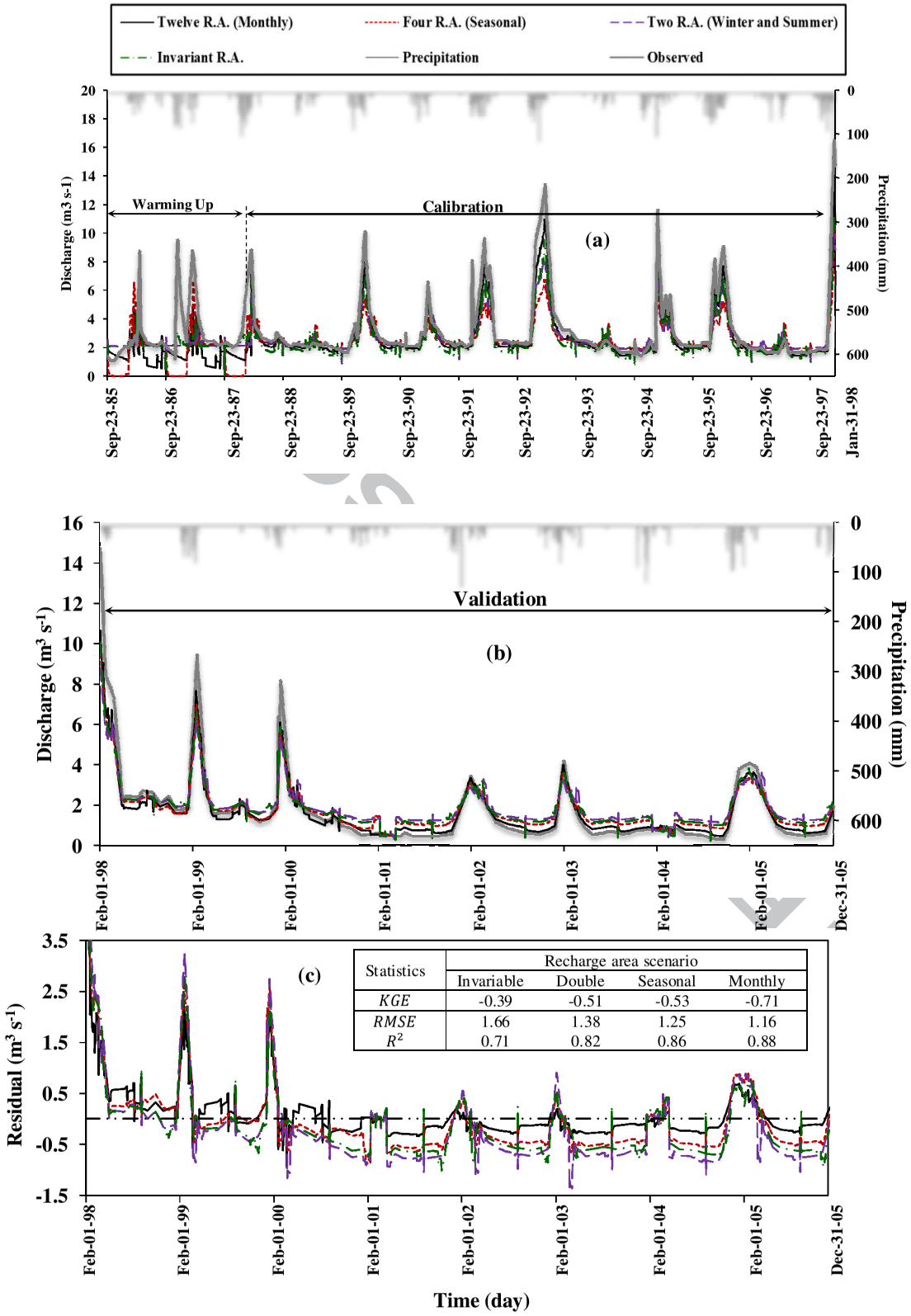

Figure (6): Observed and simulated discharge during calibration (a) and validation (b) of the proposed model considering invariable, two (Winter and Summer), four (for each season), and twelve recharge area (for each month), and residuals of the proposed model ($Q_{obs} - Q_{sim}$) obtained with different scenarios of recharge areas (c).

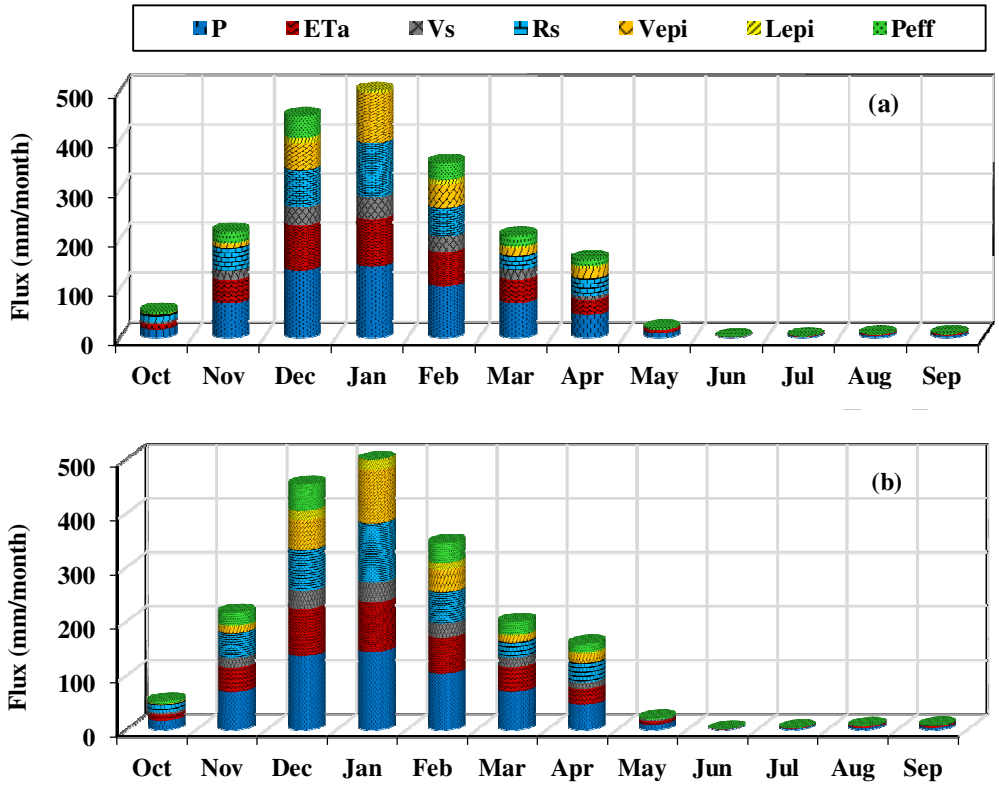

Figure (7): Water balance components estimated by the proposed model during validation period obtained with (a) invariable recharge area, and (b) monthly recharge area.

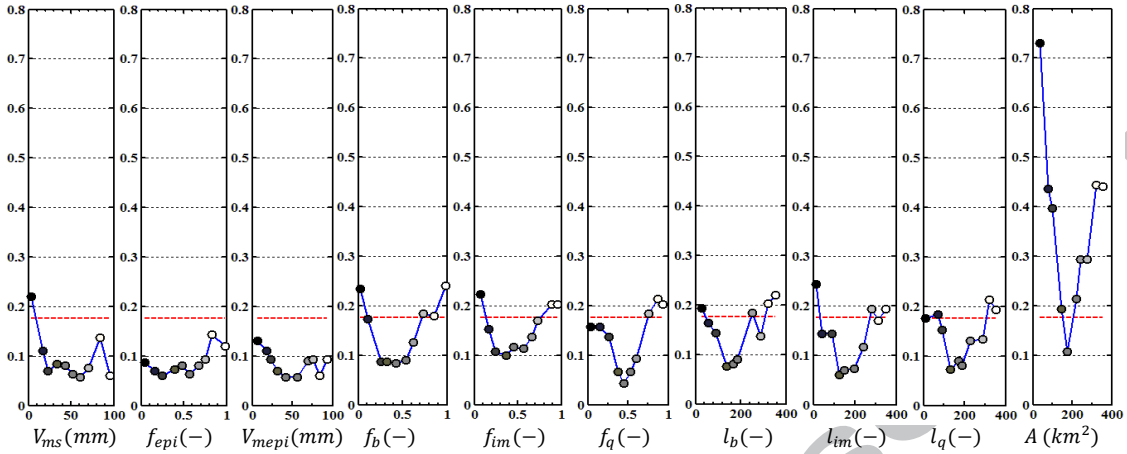

Figure (8): Kolmogorov–Smirnov statistic $\widehat{KS}$ at different conditioning values of parameters of the proposed model. The dashed horizontal line is the critical value of the KS statistic at confidence level of 0.05 *(for all cases* n = 10, N_u = 100, and N_c = 50).

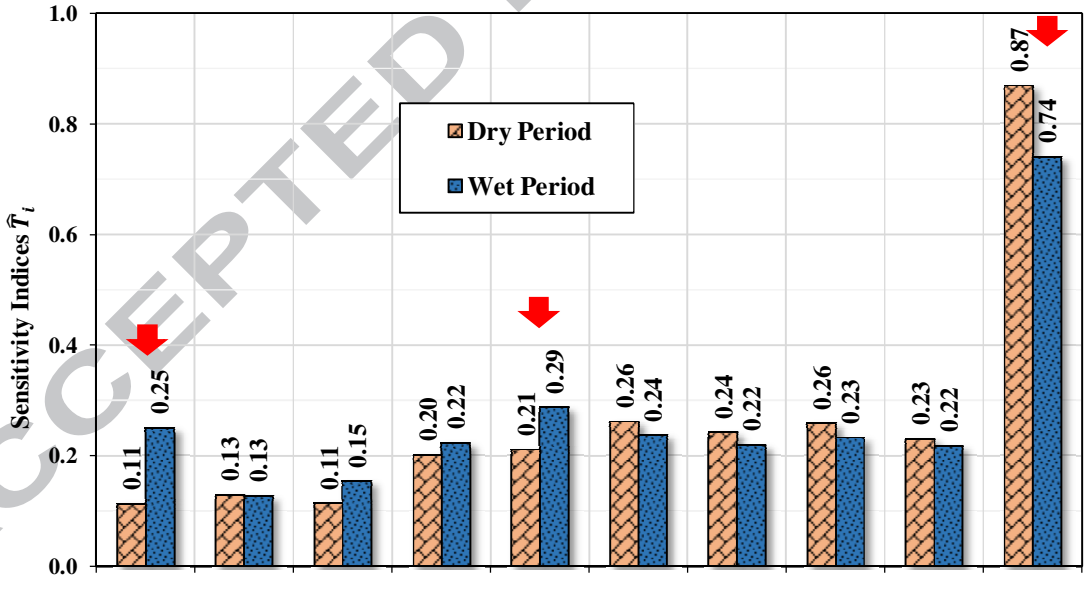

Figure (9): The sensitivity indices ($\hat{T}_i$) of the proposed model output (Q_{spring}) to the input parameters for two periods of dry and wet. Arrows indicate the $\hat{T}_i$ values with significant differences in two dry and wet periods (using t-student distribution at α=0.05.

Table (1): Parameters of developed model, description, and their ranges for calibration phase.

Parameter (Unit)	Included Sub-Model	Description	Lower Limit	Upper Limit	Time Variability
V_{ms} (mm)	SMB	Maximum soil storage capacity	0	100	Constant
V_{mepi} (mm)	EPB	Maximum epikarst storage capacity	0	100	Constant
f_{epi} (-)	EPB	Losing fraction of water stored in the epikarst	0	1	Constant
f_b (-)	GWB	Recharge fraction to base flow	0	1	Constant
f_{im} (-)	GWB	Recharge fraction to intermediate flow	0	1	Constant
f_q (-)	GWB	Recharge fraction to the fast flow	0	1	Constant
l_b(-)	GWB	Memory length of base flow	1	150	Constant
l_{im} (-)	GWB	Memory length of intermediate flow	1	150	Constant
l_q (-)	GWB	Memory length of quick flow	1	150	Constant
A (km^2)	GWB	Effective recharge area	30	350	Constant/Variable

Table (2): Results of recession curve decomposition to obtain the recession coefficients of α_b, α_{im}, and α_q.

Recession Period		$\boldsymbol{\alpha_b}$ (day^{-1})	$\boldsymbol{\alpha_{im}}$(day^{-1})	$\boldsymbol{\alpha_q}$(day^{-1})
Start Date	End Date			
29-Mar-86	06-Nov-86	0.0035	0.025	0.577
22-Feb-87	29-Oct-87	0.0021	0.0438	0.1259
22-Feb-88	04-Oct-89	0.0021	0.0192	0.256
31-Jan-90	21-Nov-90	0.0027	0.0303	0.1474
28-Feb-91	20-Oct-91	0.0024	0.0164	0.1219
15-Feb-92	04-Nov-92	0.0020	0.0972	0.2988
26-Feb-93	31-Dec-93	0.0059	0.0214	0.1637
13-Mar-94	27-Jul-94	0.0077	0.0075	0.0138
17-Apr-95	05-Sep-95	0.0020	0.0132	0.1736
12-Mar-96	31-Dec-96	0.0033	0.0188	0.1201
01-Feb-98	04-Dec-98	0.0020	0.0972	0.2985
21-Feb-99	29-Oct-99	0.0020	0.0376	0.2013
16-Jan-00	31-Dec-00	0.0059	0.0085	0.1482
03-Feb-02	02-Nov-02	0.0032	0.0209	0.0371
02-Feb-05	24-Aug-05	0.0038	0.0077	0.0352
Mean (day)		0.0033	0.0310	0.181
St. Dev. (day)		0.0018	0.0288	0.1397

Table (3): Values of the model parameters calibrated with constant, six-monthly, seasonal, and monthly recharge area through hydrological year.

Parameter (Unit)	Calibration Step			
	Invariable surface area	Surface area for Winter and Summer	Surface area for each season	Surface area for each month
V_{ms} (mm)	3.98	2.19	1.76	2.2
V_{mepi} (mm)	1.27	2.76	2.1	1.98
f_{epi} (-)	0.23	0.301	0.35	0.31
f_b (-)	0.47	0.412	0.51	0.47
f_{im} (-)	0.34	0.31	0.39	0.36
f_q (-)	0.20	0.28	0.11	0.17
l_b(-)	73	61	62	59
l_{im} (-)	26	25	30	28
l_q (-)	17	18	11	15
A (km^2)	261.78	326.54, 175.0	151.2*, 344.2, 285.3, 254.6,	314.2**, 345.2, 352.3, 336.5, 237.8, 225.4, 151.6,124.6, 125.2, 139.1, 203.1, 249.2

* These values are corresponding to season Fall, Winter, Rabbi, and Summer, respectively.

** These values are corresponding to October to September months, respectively.

Research Highlights

- Incorporating the residence time in groundwater balance model of karst aquifer.
- Temporal variations of karst recharge area are assessed on model efficiency.
- Recharge area of karst formations is the most sensitive parameter in the model.
- Intermediate flow has influential role in hydrological modeling of karst systems.